Meteorol Atmos Phys
DOI 10.1007/s00703-008-0004-5

ORIGINAL PAPER

The development of extremely dry surface air due to vertical exchanges under the exit region of a jet streak

Michael L. Kaplan · C. Huang · Y.-L. Lin · J. J. Charney

Received: 12 February 2008 / Accepted: 20 August 2008

Abstract Observations and numerical model simulations indicate that anomalous surface drying is strongly forced by mass and momentum adjustments under the right exit region of a polar jet streak overtaking and modifying a weak surface cold front. This drying event, which was associated with a wildfire in south-central New Jersey, is related to multi-scale atmospheric forcing that began far upstream and was likely not coupled to the classic cold conveyor belt model, as described by Carlson (Mon Wea Rev 108:1498–1509, 1980). The analyses indicate that both deep tropospheric circulations and boundary layer dry air advection occur in tandem to create a favorable environment for two closely associated extreme surface drying events. The *first drying event* occurs when lower tropospheric air is transported downwards in the descending branch of the low-level cold front's thermally direct circulation. This low-level circulation, which is vertically separated from the upper-level jet, is still enhanced by the hydrostatic pressure rises under the velocity convergence in the equatorward exit region of the polar jet. The upper-level convergence phases with the low-level cold air advection to intensify the low-level isallobaric wind. Dry air increases at low levels in conjunction with the isallobaric divergence behind the low-level cold front. Sinking air occurs within the 100-hPa layer centered just above 900 hPa as a result of the isallobaric divergence. The shallow descending circulation within the upstream side of this low-level front produces the first injection of dry air into the surface layer independently of deep-boundary layer mixing. Surface moisture divergence and shallow sinking sustain the dry cold front in the boundary layer. The descending air in the upper tropospheric jet circulation does *not* immediately couple to the deepening boundary layer accompanying the cold front's circulation. A *second drying event* occurs at the surface shortly thereafter, when surface heating deepens the well-mixed layer, such that the boundary layer behind the low-level front (i.e., within its trailing descending air) is linked to the dry air under the jet's equatorward exit region descending branch. Thus, the first drying event is created by the low-level direct circulation in a region of isallobaric divergence, while the second drying event is created by the coupling between the upper level indirect circulation and the deepening convective boundary layer. The two dry events combine to create a favorable environment for an isolated wildfire as both dry air and increasing surface winds develop during maximum surface heating.

M. L. Kaplan (✉)
Division of Atmospheric Sciences, Desert Research Institute,
Reno, NV 89512, USA
e-mail: mike.kaplan@dri.edu

C. Huang
Climate Prediction Center, NCEP/NWS/NOAA,
Camp Springs, MD 20746, USA

Y.-L. Lin
Department of Physics and EES Ph.D. Program,
NOAA ISET Center, North Carolina A&T State University,
Greensboro, NC 27411, USA

J. J. Charney
USDA Forest Service, North Central Research Station,
East Lansing, MI 48823, USA

1 Introduction

It has long been known that the dynamic vertical coupling of dry, high isentropic potential vorticity (IPV) air exceeding 1

PVU can occur along baroclinic zones which accompany jet/front systems. This process can transport dry ozone-rich air from the stratosphere into the lower troposphere via the classic tropopause folding process (Danielsen 1968). The transport of these air parcels to the surface occurs typically within the poleward entrance region of a curved and amplifying polar jet streak, wherein significant confluent frontogenetical forcing is occurring. This forcing includes strong low-level cold air advection. The signature of the dry air is the well-known comma cloud structure in satellite imagery accompanying deep cyclogenesis. Danielsen (1968) envisioned two large secondary circulation cells, one thermally direct and one thermally indirect, that phased to produce the jet entrance region subsidence and drying.

Studies such as those by Carlson (1980) and Schultz (2001) have examined the role of airstreams associated with conveyor belts of warm and cold air in creating the unique structure of the dry slot southwest of the comma cloud associated with extratropical cyclones. These represent primary circulations that are more persistent and larger in scale than secondary circulations associated with jet streaks. Carlson discussed the importance of the cold conveyor belt that originates poleward and downstream of the surface cyclone, where air parcels are lifted under the warm conveyor belt and rotate anticyclonically as they are transported to the upstream side of the cyclone. Descent associated with anticyclonic storm relative isentropic trajectories would result in the equatorward and/or upstream transport of cold and dry air behind the departing cyclone. Schultz (2001) revisited Carlson's synoptic model and determined that the cold dry air wrapping around the mid-upper tropospheric vortex was composed of parcels whose vertical level of origin relative to the warm front or warm conveyor belt controlled their unique trajectory, thus, forcing the parcels to turn either anticyclonically or cyclonically upstream of the cyclone. Cyclonic parcel motion upstream of the cyclone within the cold conveyor belt was favored in deep closed circulation systems and anticyclonic motion in shallower broader cyclone systems. It was demonstrated in both Carlson's and Schultz's analyses that the cold conveyor belt can be a substantial source of dry air upstream and equatorward of a cyclone. However, the driest air surrounding the cyclone in Carlson's model was not directly associated with the cold conveyor belt, as it existed in a different airstream located above the surface cold front in the 700 to 500-hPa layer under the equatorward flank of the upper-tropospheric jet's confluent flow. This dry air was located in between a limiting streamline defining the upstream flank of air within the warm conveyor belt and a limiting streamline defining the downstream flank of the cold conveyor belt.

The aforementioned studies by Danielsen, Carlson, and Schultz have, therefore, all addressed the issue of cyclones and their dry-air transport mechanisms. All three studies address situations in which cold air advection and significant dewpoint depressions in the air mass tend to be collocated, thus, comprising massive dry regions accompanying synoptic scale cyclones for a substantial portion of their development and motion. However, not addressed by these studies is the question of rapid drying in warm low-level air and its relationship to cyclones and their jet/front systems. Drying in a warm environment can be far more effective at producing anomalously low relative humidity than in a cold environment. With that in mind, one could legitimately ask the following question: is there a vertical exchange mechanism within the equatorward side of the jet exit region that occurs independently of a primary circulation (such as a cold conveyor belt) that is important in transporting dry air into the boundary layer on relatively short time scales and near or ahead of the surface cold front where the environment is relatively warm? The drying near the surface cold front is not typical of the aforementioned cyclone models, as this is more often a region of precipitation and deep convection. This dry air near the surface cold front will be far removed from the deep cold core vortex near the strong synoptic scale cyclone and its associated comma cloud, thus, the effect of the drying on surface relative humidity is amplified by the relative low-level warmth near or ahead of the cold front. While this does resemble Carlson's "dry tongue" or "dry stream" under the equatorward side of the jet, he did not examine the process of how such dry air rapidly reached the surface from the middle troposphere and near the cold front. This is an important question for fire meteorology because extremely low surface relative humidity is most likely to exist where the surface temperatures are very warm, not cold as in the aforementioned paradigms for drying associated with the cold conveyor belt or under the tropopause fold in the poleward entrance region of a jet streak.

This question is likely an important one to contemplate during the precursor period to erratic blowup fire events. It is often observed that extreme fire behavior occurs immediately behind or just ahead of a surface cold front downstream from a synoptic scale ridge of high pressure, and generally not in the immediate location of deep synoptic scale cyclogenesis and cold surface air. Brotak and Reifsnyder (1977) analyzed 52 case studies of explosive fire development in the USA and found that, in 75% of the events, the upper tropospheric flow regime was characterized by troughs with weak surface cyclones. The fires most often occurred near the surface front and in proximity to the 500-hPa trough, which was not a sharply delineated trough, nor did it contain a deep cold core vortex structure. The explosive fire development case studies analyzed by

Brotak and Reifsnyder (1977) were typically associated with weak cyclones, broad upper-level troughs, rapid boundary layer warming, drying, and the onset of gusty surface wind regimes near the surface cold front well downstream from the jet entrance region and not closely coupled to strong cold air advection, as in the cold conveyor belt model. Kondo and Kuwagata (1992) noted a similar synoptic scenario in an explosively developing wildfire case study in Japan, as did Simard et al. (1983) for the Mack Lake (1980) fire in Michigan.

Highly detailed studies of dry air accompanying surface cold fronts arriving in the immediate prefire environment have been carried out in Australia by Mills (2005a, b). Employing model-simulated fields as well as surface, satellite, and rawinsonde observations, Mills performed in-depth analyses of individual extreme drying events and also examined the climatological data of numerous prefire environments. He focused on the so-called "cool change" environment when a cold front arrives from the south or southwest along the Australian southern and southwestern coasts and propagates northeastwards along the coast, bringing extreme drying and rapid increases in surface wind gustiness conducive for the development of blowup fires. His analyses show some fairly consistent signals accompanying these surface fronts and their rapid drying. First, aloft, there is typically a massive ridge of high pressure over Australia, with a trough to the southwest of the continent. Embedded within the trough is a jet streak with its highly ageostrophic exit region propagating northeastwards. The ageostrophic vector is directed equatorwards of the isoheights in the exit region. This would create a region of velocity convergence aloft over the southwestern part of coastal Australia. Beneath this feature is a region of significant pressure rises at the surface through the planetary boundary layer with increasing cross-isobaric flow directed towards the northeast, low-level cold frontogenesis, dry air advection, and surface sensible/diabatic heating within the deepening convective boundary layer. The pressure rises typically dominate the mean sea level pressure change field, although a signal of surface cyclogenesis does also typically exist. Mills' simulations have indicated that a direct circulation cell accompanying the cold front exists, leading to strong sinking motions just behind/upstream of the region of surface frontal strengthening and motion. Mills has hypothesized that this represents the classic drying and wind-generational situation preceding most major blowup fires, with the extreme drying occurring well downstream from the jet entrance region aloft and close to the boundary layer cold or dry frontogenesis, which often maximizes around 850 hPa. The sinking cell with the boundary layer frontogenesis transports dry air surfacewards as the surface heating deepens the convective boundary layer. His climatological analyses indicated that this 850-hPa frontogenesis was the most highly correlated feature with the prefire environment and, therefore, may be a useful predictor of this environment. However, he has not synthesized the jet, low-level frontogenesis, and drying together into one coherent circulation paradigm which couples upper-level and lower-level mass, momentum, thermal, and dry air adjustments. Uccellini and Johnson (1979) have shown how a secondary sinking circulation cell can develop within the equatorward exit region of a balanced straight jet streak, although this mechanism is rarely, if ever, associated with anomalously dry air near the surface, such as is observed before major blowup fires.

This mechanism of rapid warming and drying near a surface cold front is poorly understood and needs to be addressed to improve forecasts of fire weather potential. From a broader atmospheric context, this could be another mechanism for deep vertical exchange processes that rapidly links the free troposphere and boundary layer, not dissimilar to that involving tropopause folding, which links the stratosphere and free troposphere. Thus, it could represent an important mechanism causing air to be exchanged vertically, resulting in the transport of constituents into and out of the convective boundary layer.

In this paper, we diagnose the interactions among multiscale dynamical processes that we hypothesize have resulted in the rapid vertical transport of warm, dry, and high momentum air from the middle troposphere to the vicinity of a surface cold front and low-pressure trough. The fire weather case study of interest is the 2nd June 2002 "Double-Trouble" (DT) fire in coastal central New Jersey (e.g., Charney et al. 2003; NJFFS 2003), wherein transient and localized fire weather conditions, i.e., anomalously dry surface air and gusty surface winds, presented a major challenge for fire weather forecasting. The DT fire occurred between Atlantic City, NJ (KACY) and New York City (KOKX). The airmass drying just preceding the fire was anomalous for New Jersey in June, with observed surface relative humidity $<20\%$ accompanied by gusty surface winds of ~ 17 m/s and surface temperatures $>30°C$. The fire was localized to the State Park and occurred primarily between 17.00 and 20.00 UTC (13.00 and 16.00 EDT) in the immediate post surface cold frontal environment (e.g., Charney et al. 2003). The fire spread from the State Park across the Garden State Parkway and into a nearby residential neighborhood, necessitating the closure of the nearby Garden State Parkway and producing a major impact on transportation and public safety.

We will employ both observations and numerical simulations to describe several stages of an original paradigm that represents the mechanism by which weather conducive to extreme fire behavior develops in this case study. Section 2 of this paper will detail the observational

evidence for pronounced surface ridging and drying beneath an upper-level jet's equatorward exit region. In Sect. 2 will be presented the evidence for surface drying signals and the location of drying relative to the larger scale advection of cold and warm air. Section 3 will describe the numerical model experiment and a brief model validation. Section 4 will employ data from a numerical simulation experiment to describe meso-α–meso-β scale adjustments not well-observed in the relatively coarse observational datasets, starting with the first drying episode/mechanism and ending with the second drying episode/mechanism. Section 5 will summarize the results.

2 Surface and upper-air observations of precursor multi-scale processes leading to anomalous drying over the New Jersey Coastal Plain

2.1 Synoptic scale circulations upstream from dry air arriving near DT

Figure 1a–d depicts the 875-hPa temperatures and winds, as well as the 875-hPa relative humidity and height data derived from the North American Regional Reanalysis (NARR-A) (e.g., Mesinger et al. 2006) dataset valid at 12.00 and 15.00 UTC 2nd June 2002. 875 hPa was selected because it is very close to the level of maximum sinking air velocity near DT during this time period in the NARR analyses (Fig. 1e). Evident is a deep 875-hPa cyclone over Labrador with a broad trough extending southward along the Atlantic coast to New Jersey (NJ) and Pennsylvania (PA). The cold pool of air over eastern Canada, the northern Great Lakes, and New England at 875 hPa can be seen in Fig. 1c, d. Also depicted in these figures is a wind shift line (thick dashed) that reaches NJ by 15.00 UTC from its western PA location at 12.00 UTC. This wind shift line separates predominantly downstream west-northwesterly from upstream northwesterly air flow at 875 hPa, as well as serving as a boundary of slightly colder air advecting from the west-northwest. Note that the lowest 875-hPa heights are nearly 1,500 km to the northeast of the location of DT (see Fig. 2a for DT's location), the highest 875-hPa heights are located a similar distance upstream over Minnesota, and also that the 875-hPa flow vectors are only slightly crossing the isotherms over southern NJ at 15.00 UTC, indicating weak cold air advection. Of most importance is the location of the driest air at 875 hPa, which is south and west of DT at 15.00 UTC, near the southeastern PA/southwestern NJ border.

Depicted in Fig. 2b and c are important observations at KACY and Sandy Hook, NJ, near DT, indicating the explosive local drying signal embedded within the aforementioned synoptic scale features. In Fig. 2b is the dewpoint trace in the meteogram at KACY, located only ~35 km to the south-southwest of DT and in Fig. 2c is the GPS integrated precipitable water trace ~35 km to the north-northeast of DT at Sandy Hook. Both figures show rapid and dramatic drying signals. This drying amounts to a >15°C dewpoint reduction at KACY and a >1.5-cm integrated precipitable water reduction at Sandy Hook within the 15.00–18.00 UTC period just following the 875-hPa wind shift line passage in Fig. 1b. The drying lasts ~3 h at both locations and there is evidence of a double pulse of drying (nos. 1 and 2), with the second pulse's drying rate being more pronounced. Additionally, at KACY, only minimal cooling accompanies the wind shift line passage from the west-northwest to the northwest, which follows the early afternoon warming, with temperatures rapidly rising to ~31°C before 17.00 UTC and then slowly falling from ~31°C after 17.00 UTC.

The sinking motion behind the wind shift line at 875 hPa can be seen in Fig. 3a and b over most of the Delaware River Valley, NJ, and eastern/south-central PA at this time. This descent extends west-southwestward across much of PA by 15.00 UTC. There is also developing 875-hPa velocity divergence spanning the same time period in Fig. 3c and d arriving just west of NJ in eastern PA behind the wind shift line at 15.00 UTC. Surface wind shifts from predominantly westerly at 15.00 UTC to west-northwesterly at 18.00 UTC are occurring at KACY in Fig. 2b and also in the New Brunswick, NJ wind profiler near Sandy Hook at the same time from the surface to 2.5-km elevation (not shown). This uniform 2.5-km depth is consistent with NARR-A planetary boundary layer (PBL) depths between 2 and 2.5 km over New Brunswick at 18.00 UTC (not shown). The first pulse of surface drying in Fig. 2b and the 875-hPa cold air advection in Fig. 1d are closely phased at 15.00 UTC. Thus, the observed drying is very pronounced over NJ in conjunction with the arrival of a weak surface cold front; however, the surface temperatures drop very little while this drying is occurring. This drying with weak boundary layer cold air advection is occurring nearly 1,500 km from the synoptic scale low-pressure center ~984 hPa located to the northeast and the dry air is transported into DT predominantly from the west.

2.2 Subsynoptic scale dry air transport and related circulations

In this section, we will provide observational evidence describing the synoptic and finer scale processes associated with the dry air transport and dynamics during and preceding the same time period diagnosed in the previous subsection. Figures 4a–c and 5a–c depict the sequence of surface dewpoint depression and surface mixing ratio/surface winds valid from 12.00 to 18.00 UTC for the dewpoint

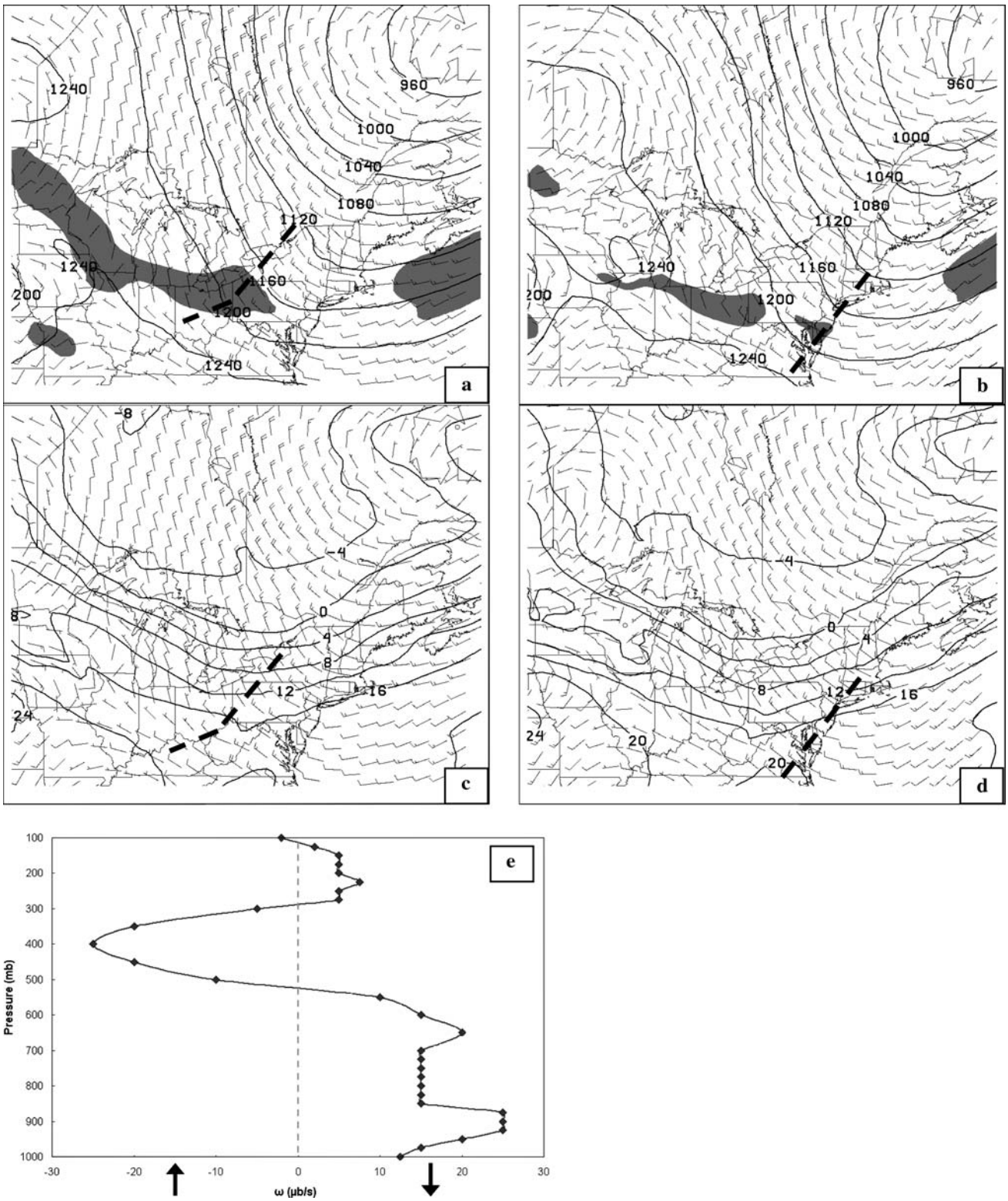

Fig. 1 North American Regional Reanalysis (NARR-A) 875-hPa height (m), wind barbs (long barb = 10 kt and short barb = 5 kt), and relative humidity (shaded <40%) valid at **a** 12.00 UTC and **b** 15.00 UTC 2nd June 2002. NARR-A 875-hPa temperature (°C) and wind barbs (kt) valid at **c** 12.00 UTC and **d** 15.00 UTC 2nd June 2002. The *bold dashed line* represents the wind shift line location. **e** NARR-A vertical profile of omega (μb/s) at Double-Trouble (DT) valid at 15.00 UTC 2nd June 2002

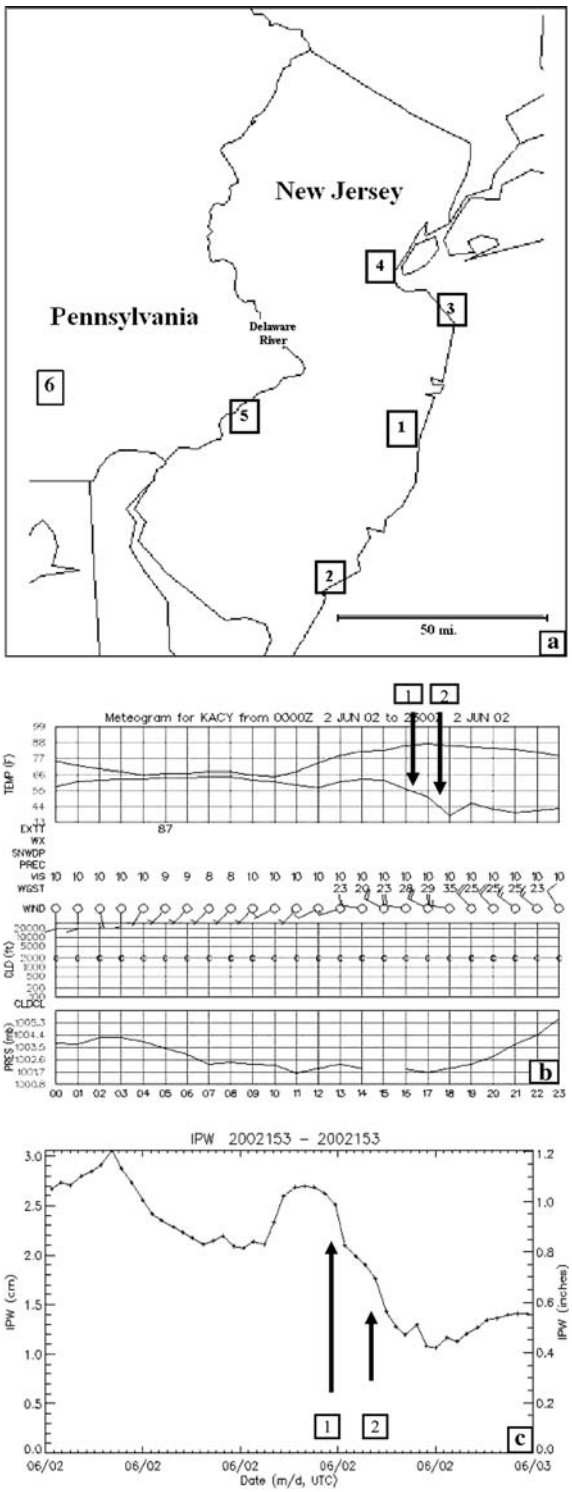

Fig. 2 **a** Map depicting locations in New Jersey, including (*1*) Double-Trouble State Park, (*2*) Atlantic City, (*3*) Sandy Hook, (*4*) New Brunswick, (*5*) Delaware River, and (*6*) Harrisburg, PA. **b** Surface meteogram at Atlantic City, New Jersey (KACY) valid from 00.00 UTC 2nd June to 23.00 UTC 2nd June 2002. **c** Observed global positioning system (GPS) integrated precipitable water at Sandy Hook, New Jersey, valid from 00.00 UTC 2nd June to 00.00 UTC 3rd June 2002. The *arrows* (*1* and *2*) point to the middle of the period of the two main drying episodes

depression, the winds, and the mixing ratio. Upstream and just before 12.00 UTC, a maximum in the surface dewpoint depression of ~12°C is located just northwest of Holland, Michigan (MI) (BIV) at 06.00 UTC (not shown), which moves east-southeastwards to be located just east of BIV by 09.00 UTC (not shown). Then, the maximum begins to intensify to >14°C just northwest of Pittsburgh, PA (PIT) by 12.00 UTC (Fig. 4a), to just northwest of and, subsequently, over Harrisburg, PA from 12.00 to 15.00 UTC (Fig. 4a, b), to between HAR and Philadelphia, PA (PHL) from 15.00 to 18.00 UTC (Fig. 4b, c), and near KACY by 18.00 UTC (Fig. 4c), nearly coincident with the dry swath at 875 hPa in Fig. 1a and b. This surface dewpoint depression maximum intensifies to ~22°C and expands over area in time as it is embedded within and oriented the same as the slow predominantly southward moving surface baroclinic zone (note Figs. 1c, d, 6, 9 and 12c, d), which is very close to the south–north mixing ratio gradient near the OH and PA state southern boundaries in Fig. 5a–c. The west–east swath of dry air (i.e., to be referenced as the equatorward dry pool) can be seen in Fig. 1a and b at 875 hPa and Figs. 4b, c and 5b, c at the surface as a narrow elongating feature.

The motion of the drier and equatorward surface air pool is predominantly eastward, with only a weak southward component consistent with the dominant westerly surface flow evident in Fig. 5a–c over southern PA, Maryland (MD), and NJ. These figures indicate that the dry air at the surface is elongating east-southeastward towards KACY. Also inferred from these figures and the KACY meteogram in Fig. 2b is that the dewpoint depressions in Fig. 4a–c are controlled early on (before 15.00 UTC) by dry air transport over OH and PA, followed by both dry air transport and surface heating, overwhelming the surface cold air advection over PA and NJ (during 12.00–18.00 UTC).

In Fig. 6a–i, the surface drying can be seen to be collocated with a west-northwest–east-southeast plume of low specific humidity ~200–300-km wide lying just north of the 875-hPa front in Fig. 1c and d and the meridional moisture gradient in Fig. 5a–c, extending up to 650 hPa. It covers the region from southern MI/Lake Erie to southern PA/NJ during the 12.00–18.00 UTC time period. At 875-hPa, the dry air transport is similar to that at the surface in Fig. 4a–c, with dry air transport from OH to southern NJ just north of the surface front. At 725 hPa, the dry air is slightly north of the 875-hPa swath and is being transported from Lake Huron to southeastern PA, while at 650 hPa, the transport orientation is the same as 725 hPa, yet, it is moving faster and located farther north.

The equatorward dry air pool arriving at 18.00 UTC near DT within the surface front (Fig. 4a–c) and just above it (Fig. 6a–i) is clearly transported by the west-northwesterly

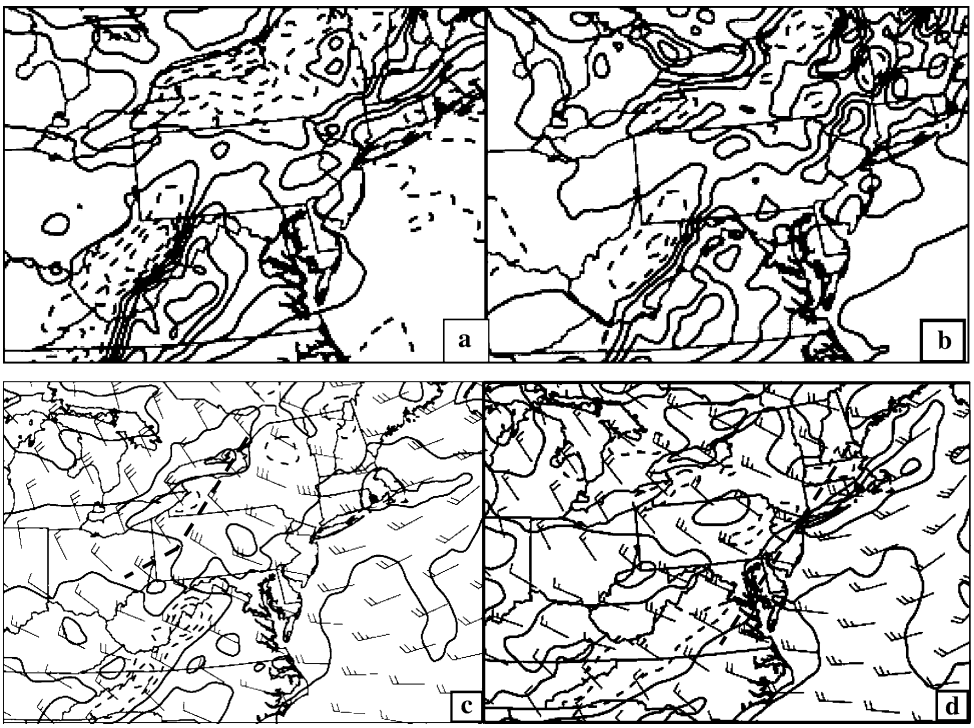

Fig. 3 NARR-A analysis of 875-hPa omegas (10^{-3} Pa/s) (positive solid beginning at 0 Pa/s and negative dashed beginning at -2×10^{-3} Pa/s; contour interval is 2×10^{-3} Pa/s) valid at **a** 12.00 UTC and **b** 15.00 UTC 2nd June 2002. NARR-A analysis of 875 hPa wind barbs (kt) and velocity convergence (positive solid beginning at 0 s^{-1} and negative dashed beginning at -30×10^{-6} s^{-1}) valid at **c** 12.00 UTC and **d** 15.00 UTC 2nd June 2002. The *bold dashed line* represents the wind shift line location

flow within the lower troposphere. The northwesterly flow on the immediate west side of the Labrador low above 875 hPa extends down to the Canadian border well northeast of this dry air that affects DT, although it likely is affecting the second separate poleward dry air pool north and east of Lake Ontario (Figs. 4c and 9a–c).

Figure 7a–h depicts a sequence of NARR 500-hPa winds, heights, and omegas from 06.00–15.00 UTC. At 15.00 UTC, 500 hPa represents the level of convergent air flow supporting a strong sinking maximum seen just below 600 hPa in Fig. 1e. These figures depict the motion of the 500-hPa jet exit region, the strongest equatorward-directed ageostrophic wind vector, as well as the vertical motion during this period of rapid east-southeastward-directed drying within the lower troposphere evident in Figs. 4a–c, 5a–c, and 6a–i. One can diagnose the motion of the equatorward-directed ageostrophic flow vector relative to the sinking motion in the jet exit region in Fig. 7a–d. The thick arrow highlights the location of the maximum ageostrophic vector, which is located over northern Ohio southeast of the >40-m/s winds at 06.00 UTC. It propagates over southwestern PA by 09.00 UTC in Fig. 7b, near the central PA/MD border by 12.00 UTC in Fig. 7c, and southeastern PA/eastern MD by 15.00 UTC in Fig. 7d. This motion and the trailing descending air in the accompanying omega fields in Fig. 7e–h are juxtaposed with the aforementioned drying in Figs. 4, 5 and 6 as the ageostrophy and descent lie within the sloping dry zone from the surface front to 650 hPa extending from southern MI/OH to MD/southern NJ. Much of this occurs on the windward side of the mountains. Thus, the motion of the dewpoint depression maximum and mixing ratio minimum from the surface to $\sim$650 hPa is closely correlated with the descent and velocity convergence on the equatorward side of the midtropospheric jet's right exit region.

A simple moisture budget calculation was performed employing NARR-A data over DT at 15.00 UTC within the layer centered on $\sim$875 hPa. The specific humidity divergence of $\sim 10^{-7}$ kg/kg, zonal advection of specific humidity $\sim -13 \times 10^{-8}$ kg/kg, meridional advection of specific humidity $\sim 8 \times 10^{-8}$ kg/kg, and the 850–900-hPa vertical advection of specific humidity $\sim -25 \times 10^{-8}$ kg/kg were calculated at DT. This simple budget yields decreasing values of specific humidity due to three-dimensional advection $\sim -30 \times 10^{-8}$ kg/kg at DT at 15.00 UTC and highlights the importance of sinking motions and zonal advection in transporting lower-mid-tropospheric dry air into the PBL corresponding to the onset of the first rapid drying episode in Fig. 2b. These two sources contributed to a reduction of the specific humidity by $\sim 1.1 \times 10^{-3}$ kg/kg h^{-1}, consistent with Fig. 6a and b. Turbulent fluxes of moisture were not available from NARR for comparison within the budget calculations; however, the NARR-A PBL depth at 15.00 UTC exceeded 2 km, indicating that vertical mixing was potentially a developing factor in this process.

Additionally, the mean sea level pressure tendency and 875-hPa thermal advection fields in Fig. 8a–f indicate that

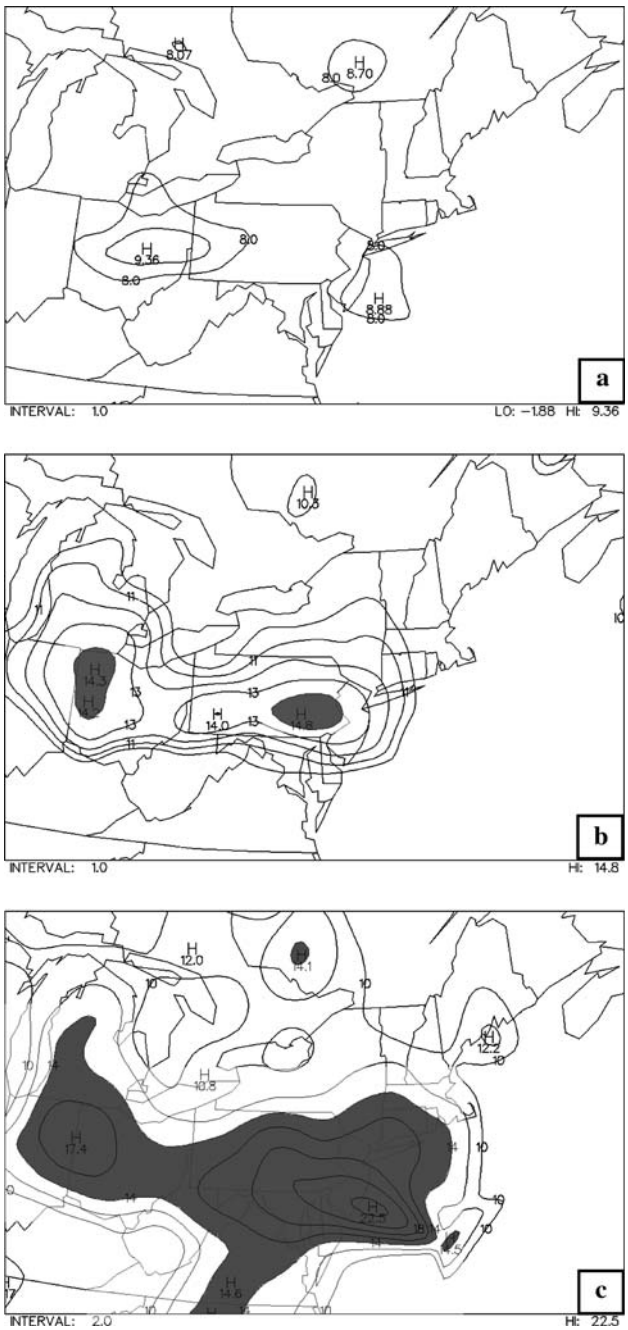

Fig. 4 Analyzed surface dewpoint depression >10°C (shaded > 14°C) valid at **a** 12.00 UTC (shown for dewpoint depression >8°C), **b** 15.00 UTC, and **c** 18.00 UTC 2nd June 2002

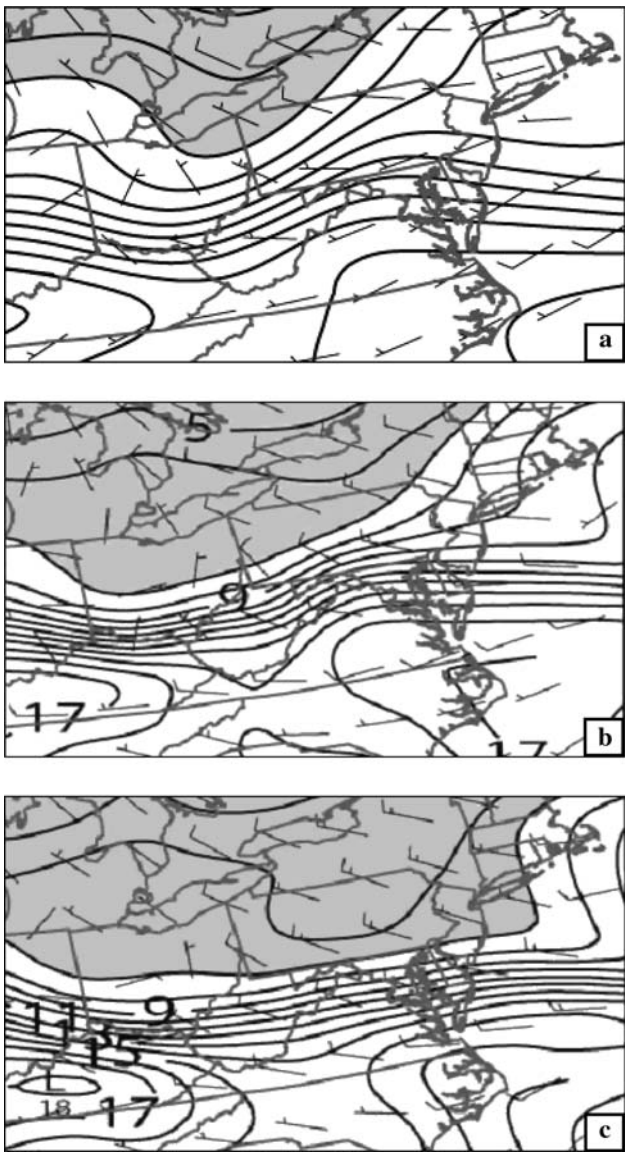

Fig. 5 NARR-A analysis of the surface mixing ratio (g/kg) and surface wind barbs (kt) valid at **a** 12.00 UTC, **b** 15.00 UTC, and **c** 18.00 UTC 2nd June 2002 and shaded below 7 g/kg

the strongest surface pressure rises occur just west of this propagating exit region at 09.00 UTC in Ohio in Fig. 8a, at 12.00 UTC in western PA and New York (NY) in Fig. 8b, and at 15.00 UTC in west-central PA in Fig. 8c, close to the largest descending motion at 500 hPa in Fig. 7e–h. When the 875-hPa temperature advection in Fig. 8d–f is compared to the pressure tendency fields in Fig. 8a–c, one can see a decoupling of cold air advection maxima from these pressure tendency maxima in time. This decoupling is the result of the cold air advection maxima leading the pressure rise maxima. It is closely coupled to the 875-hPa wind shift line/weak cold front described in the previous subsection in Fig. 1a–e, indicating multiple regions and forcing mechanisms of integrated column mass flux convergence.

2.3 Discussion of observations

The synoptic and subsynoptic fields depicted in Figs. 1, 2, 3, 4, 5, 6, 7 and 8 as well as satellite imagery in Fig. 9a–c indicate important processes just upstream from the rapid surface drying at KACY and rapid column drying at Sandy Hook between 15.00 and 18.00 UTC. These data indicate

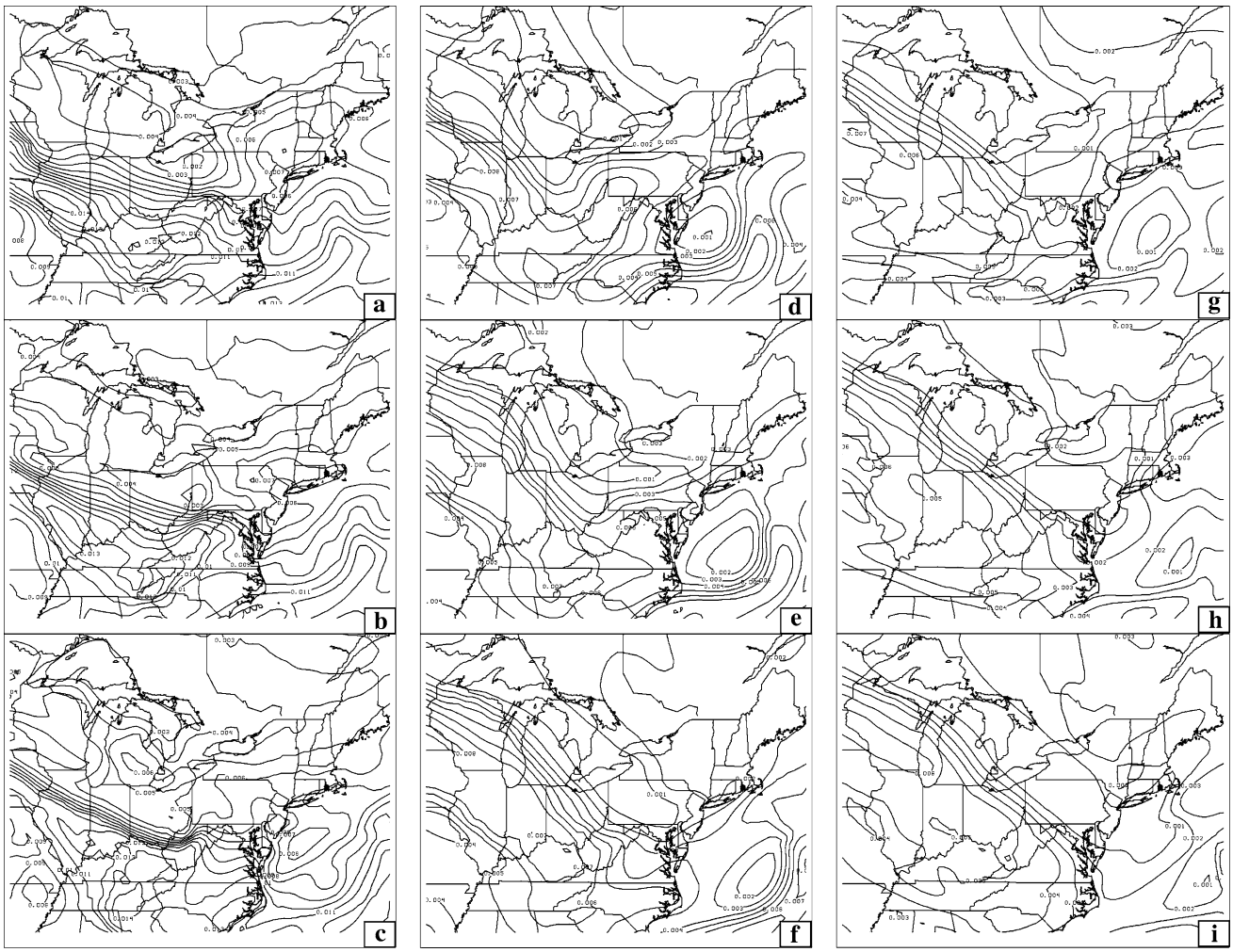

Fig. 6 NARR-A analysis specific humidity (kg/kg) valid at **a–c** 875 hPa, **d–f** 725 hPa, and **g–i** 650 hPa for 12.00, 15.00, and 18.00 UTC 2nd June 2002

that the lower tropospheric drying is closely juxtaposed to the propagating jet exit region's equatorward quadrant as the ageostrophic flow and mid-tropospheric sinking occur above the west–east swath of low-level dry air approaching DT from the west-northwest. This dry air extends through the column from the surface to 650 hPa. Not only are there two surges of drying near DT, but over the entire north-eastern US region, the satellite imagery (Fig. 9a–c), dewpoint depressions (Fig. 4a–c), and 650-hPa specific humidity (Fig. 6g–i) all support two different locations of dry tongues between 14.00 and 18.00 UTC. Visible in the clearing (dark) swaths in time in Fig. 9a–c is one dry (poleward) tongue (northern arrow) oriented parallel to the 875-hPa airflow and located to the northwest of DT over Ontario and upstate NY closer to the surface low and large cold pool aloft depicted in Fig. 1c and d. Also visible is a second (equatorward) dry tongue (southern arrow) that extends from northern-central PA to northern Virginia (VA) to southern NJ near DT, and strengthens in time along the leading edge of the cold air at the surface. The poleward dry swath is coincident with the broader synoptic scale cold air advection pattern as it is embedded in the deep cold air layer equatorward and west of the cyclone, as well as poleward of the polar jet exit region. It is also collocated with an upper tropospheric maximum of IPV (not shown) moving southeastward from Ontario. The equatorward dry tongue is on the opposite side of the jet exit region wind maximum from the IPV maximum and in much weaker cold air advection coincident with the low-level west–east cold front. Thus, the observations indicate a substantial separation of dry tongues between the: (1) synoptic scale forcing signal poleward of the jet closer to the deep cold vortex and (2) the subsynoptic scale forcing signal equatorward on the anticyclonic side of the jet exit region.

Additionally, the drying upstream from and eventually arriving near DT at the surface and immediately above the surface is well established 6–12 h before 18.00 UTC (DT

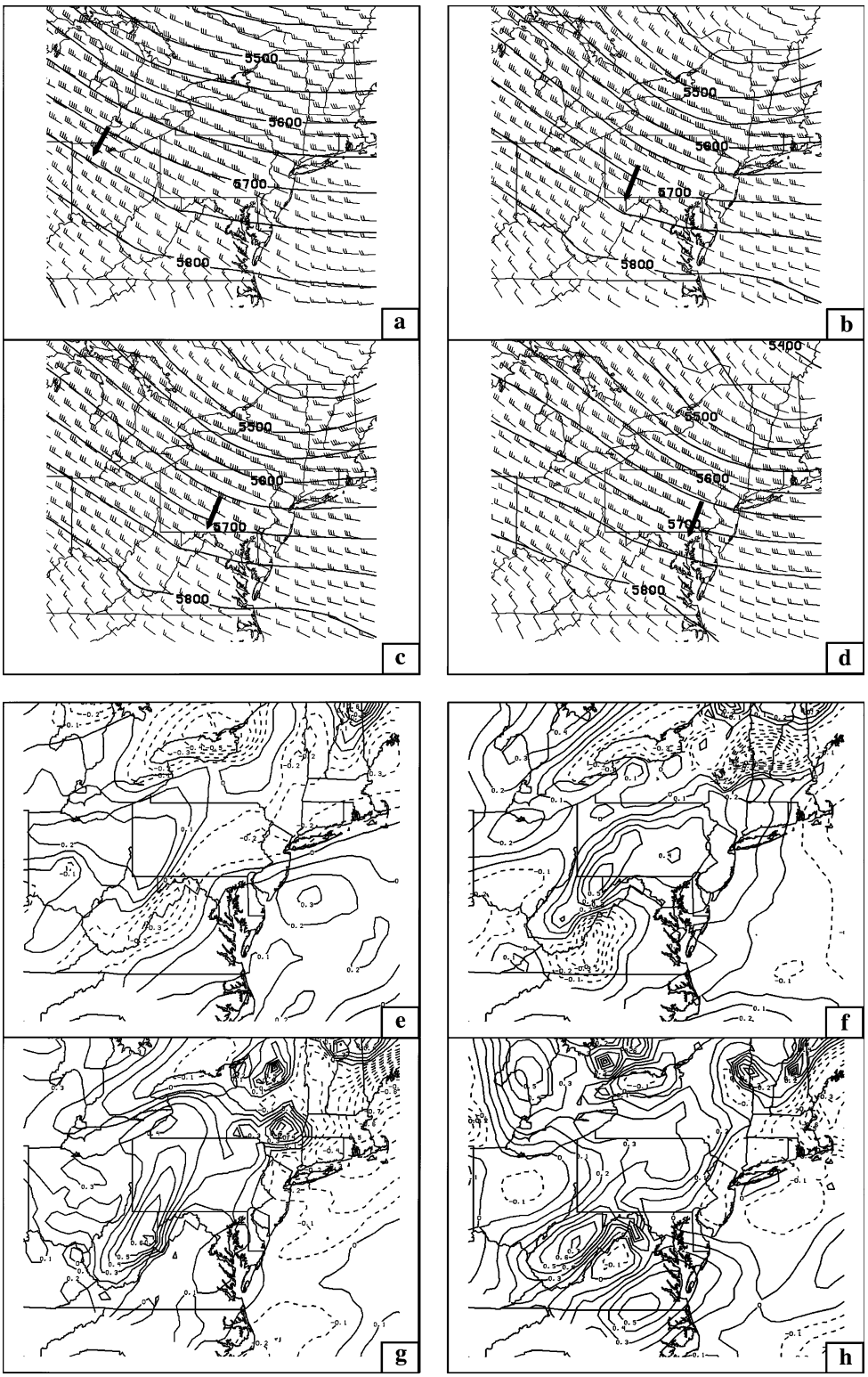

Fig. 7 NARR-A analysis of 500-hPa winds (kt), heights (m), and location of the most significant ageostrophic wind vector (*arrow*) valid at **a** 06.00 UTC, **b** 09.00 UTC, **c** 12.00 UTC, and **d** 15.00 UTC 2nd June 2002. NARR-A analysis of 500-hPa omegas (10^{-3} Pa/s) (positive solid beginning at 0 Pa/s and negative dashed beginning at -2×10^{-3} Pa/s) valid at **e** 06.00 UTC, **f** 09.00 UTC, **g** 12.00 UTC, and **h** 15.00 UTC 2nd June 2002

fire time), as is evident in Figs. 4, 5 and 6, even though it strengthens in time as the dewpoint depression maximum approaches the crest and lee slope of the Appalachian Mountains. The upstream drying that arrives near DT is also established in proximity to the anticyclonic side of the jet and originated much earlier near a massive ridge west of the Great Lakes, which was well displaced from the cold air pool over northeastern Canada (Fig. 1a–d). This assertion can be further supported by the soundings in Fig. 10a–c at Dulles, VA (KIAD), PIT, and KOKX. All

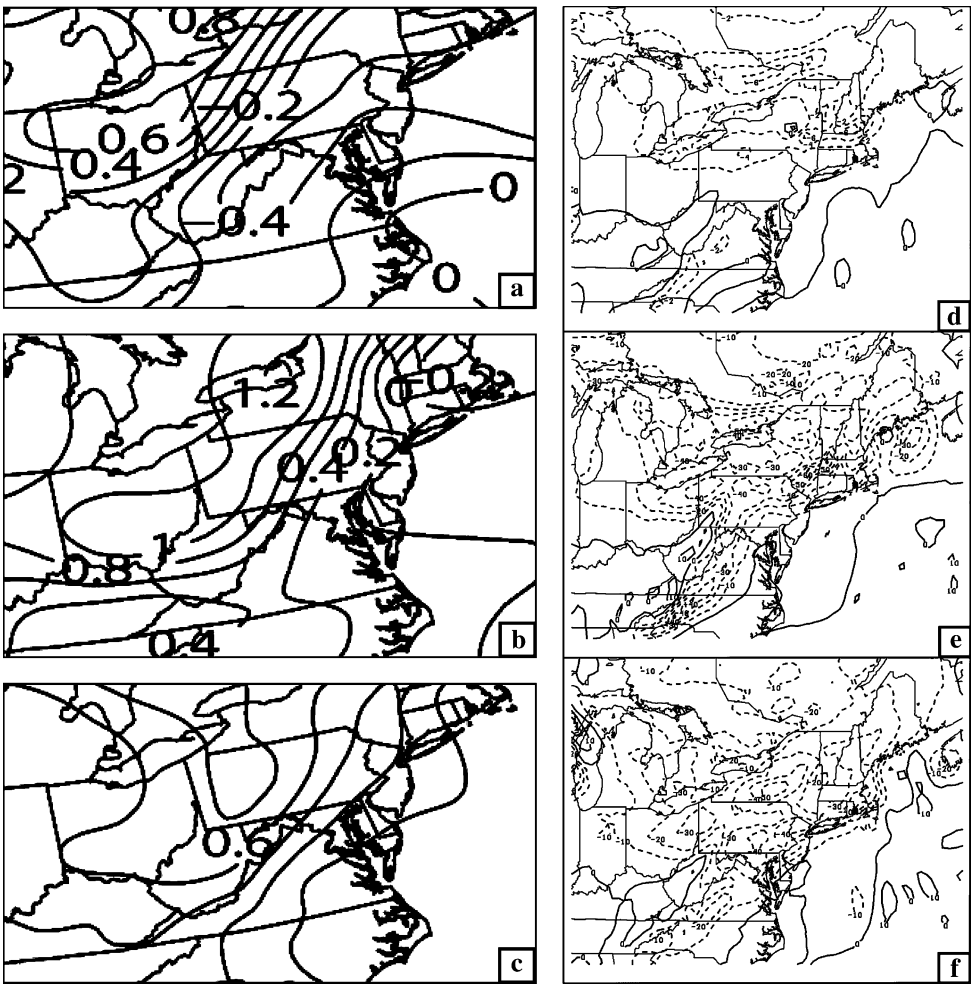

Fig. 8 Analyzed observations of hourly surface mean sea level pressure tendency (hPa) valid at **a** 09.00 UTC, **b** 12.00 UTC, and **c** 15.00 UTC 2nd June 2002. NARR-A analysis of 875-hPa thermal advection (positive solid and negative dashed in °C/h) valid at **d** 09.00 UTC, **e** 12.00 UTC, and **f** 15.00 UTC 2nd June 2002

soundings exhibit very dry layers between ~850 and 950 hPa at 12.00 UTC, independently of their location upstream or downstream from the Appalachian lee slope. They also exhibit signals of elevated adiabatic layers immediately above the dry lower layer. The adiabatic layers extend close to a second upper dry layer between 600 and 700 hPa at KIAD and PIT. As can be seen in Fig. 1e, the 900- and 650-hPa levels are regions of substantial descent consistent with the rawinsonde dry layers. These dry layers are also well equatorward and west of the poleward dry tongue in the cold air advected southeastward from Ontario to upstate NY evident in Fig. 9a–c. In the next section, model simulations will be employed to further delineate these details and enhance our understanding of the mesoscale processes inferred from the observations.

3 Model simulation experiment and validation

In order to diagnose in more detail the multi-scale adjustment processes that focus dry air near DT during the afternoon fire period, particularly the upper-level mesoscale processes that are not well-observed, a series of numerical simulation experiments were performed. The numerical simulations were performed with the Non-Hydrostatic version of the Mesoscale Atmospheric Simulation System (NHMASS version 6.3). Details of the hydrostatic model version can be found in Kaplan et al. (2000). The nonhydrostatic version employs the same physics as the hydrostatic version, with the exception of a turbulence kinetic energy planetary boundary layer scheme developed by Therry and Lacarrère (1983). Simulations were performed with 32-, 8-, and 2-km horizontal grid spacing and one-way grid nesting. The matrix sizes were comprised of $120 \times 120 \times 59$, $140 \times 140 \times 59$, and $150 \times 150 \times 59$ grid points for the 32-, 8-, and 2-km spacings, respectively. The three simulations were initialized at 00.00 UTC, 09.00 UTC, and 15.00 UTC 2nd June 2002, respectively. The regions of integration are depicted in Fig. 11. All simulations were integrated through to 21.00 UTC 2nd June 2002, with the period between 17.00 and 20.00 UTC being the key time period for assessing fire weather conditions. The initial data for the coarse-mesh simulation was composed of the NWS Eta analysis with

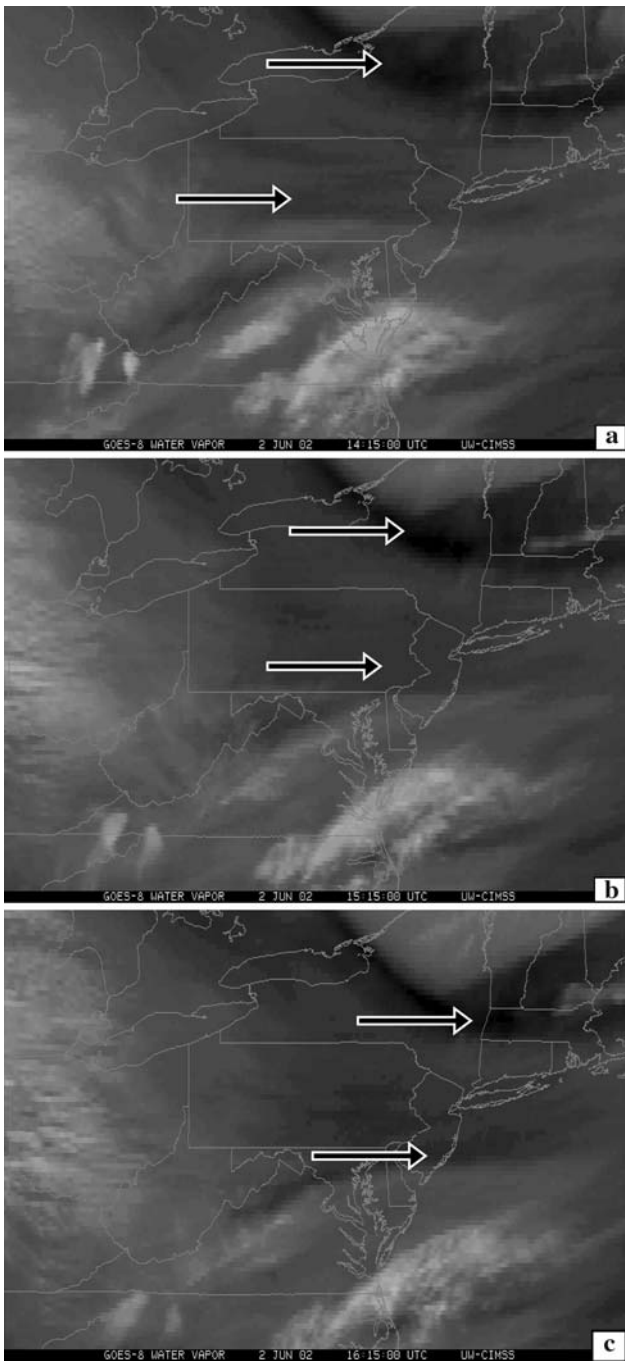

Fig. 9 GOES water vapor satellite imagery valid at **a** 14.15 UTC, **b** 15.15 UTC, and **c** 16.15 UTC 2nd June 2002. The *arrows* indicate the changing location of the dry tongues

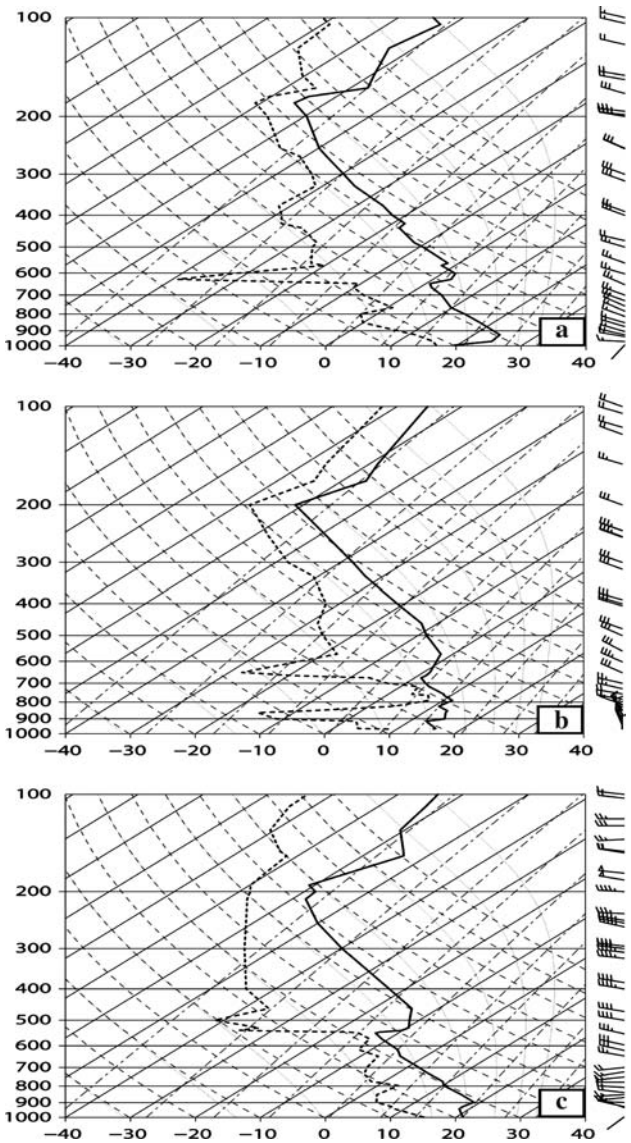

Fig. 10 Skew-t rawinsonde soundings valid at 12.00 UTC 2nd June 2002 for **a** Dulles, Virginia (KIAD), **b** Pittsburgh, Pennsylvania (KPIT), and **c** New York, New York (KOKX)

reanalyzed rawinsonde and ASOS observations. Time-dependent lateral boundaries for the coarse-mesh simulation were derived from the Eta model analysis fields, while each nested grid was initialized with cubic spline interpolated larger scale data. Time-dependent datasets for each nested grid lateral boundary condition were based on the next coarser grid's simulated dependent variables. Climatological June sea surface temperatures were assumed in the simulations. For soil moisture, 0.5° latitude and longitude 50-year average June precipitation and temperature data over the location of the simulations were employed to develop a database of representative values.

Before describing the NHMASS-generated mesoscale fields, evidence is presented to validate the general synoptic structure of the 00.00 UTC initialized 32-km simulation at DT just before and during the observed extreme drying period coincident with the fire. Figure 12a depicts the 32-km simulated sounding valid at DT at 12.00 UTC 2nd June. The key features are a nearly dry adiabatic layer between the surface and just below 700 hPa, as well as extremely dry air with dewpoint depressions $\sim$20°C below 950 hPa, as well

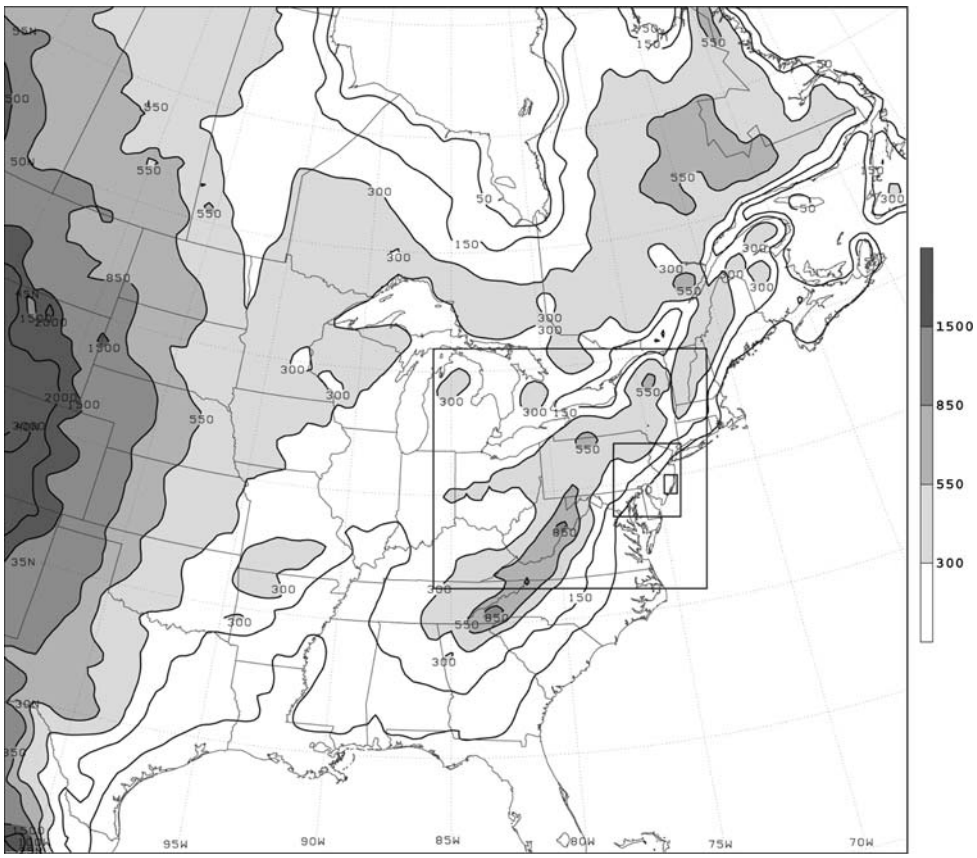

Fig. 11 Multi-scale grid locations for the 32-, 8-, and 2-km numerical simulation experiments superimposed on the coarse-resolution terrain (m)

as between 500 and 700 hPa. A uniform west-northwesterly wind flow exists up to ~700 hPa, with more westerly flow immediately above that level. Figure 12b depicts the NWS ETA analysis sounding at the same time and location for comparison, which indicates similar features. The simulated and observed 1,000-hPa temperature fields in Fig. 12c and d indicates a warm tongue of air just east of the Appalachian Mountains from Georgia to Maine (where the mean sea level pressure is very close to 1,000 hPa, e.g., 1,002 hPa at KACY and 1,002.1 hPa at KOKX, where surface elevations are <50 m), with both simulated (~27°C) and observed (~28°C) temperatures at DT being similar in between KACY and KOKX at 18.00 UTC. Near-surface west-northwesterly winds of 5–10 m/s occur just west of the cold frontal trough and confluent wind shift line. The observed (~30%) and simulated relative humidity (~25%) between KACY and KOKX in Fig. 12e and f generally matches up well; however, the offshore simulated relative humidity values are arbitrarily set to a high value over the Atlantic, Gulf of Mexico, and Great Lakes for display purposes in the postprocessor, and are not representative of the simulated fields.

Figure 12g, h depicts the NWS ETA analysis and 32-km simulated 850-hPa winds and temperatures. Figure 12i, j depicts the same fields at 500 hPa at 18.00 UTC. While the 850-hPa winds at DT are very similar, the model is slightly slow in advecting cold air over DT as the cold frontal trough propagates approximately 30–60 min too slowly in the model. A similar model error exists at 500 hPa. The 500-hPa wind speed maximum and polar jet location do match the observed data rather well, however, with both model and observations indicating a jet maximum between 40 and 50 m/s centered over southwestern Ontario (note PJ), with its equatorward exit region over eastern PA, NJ, and NY. The simulated equatorward exit region ageostrophic flow over PA and NJ is most pronounced over PA. Since the 500-hPa height and temperature isolines are nearly identical in orientation, one can infer the equatorward-directed ageostrophy at 500 hPa over PA. From a synoptic perspective, the main deficiency of the model simulation is its slow speed. However, the sounding structure, 500-hPa jet, and surface moisture and temperature fields closely replicate the observed analyses over southern NJ, which is necessary if credibility is to be established for the finer scale simulations of the equatorward exit region, low-level frontal structure, and the unstable boundary layer development and structure between 12.00 and 18.00 UTC.

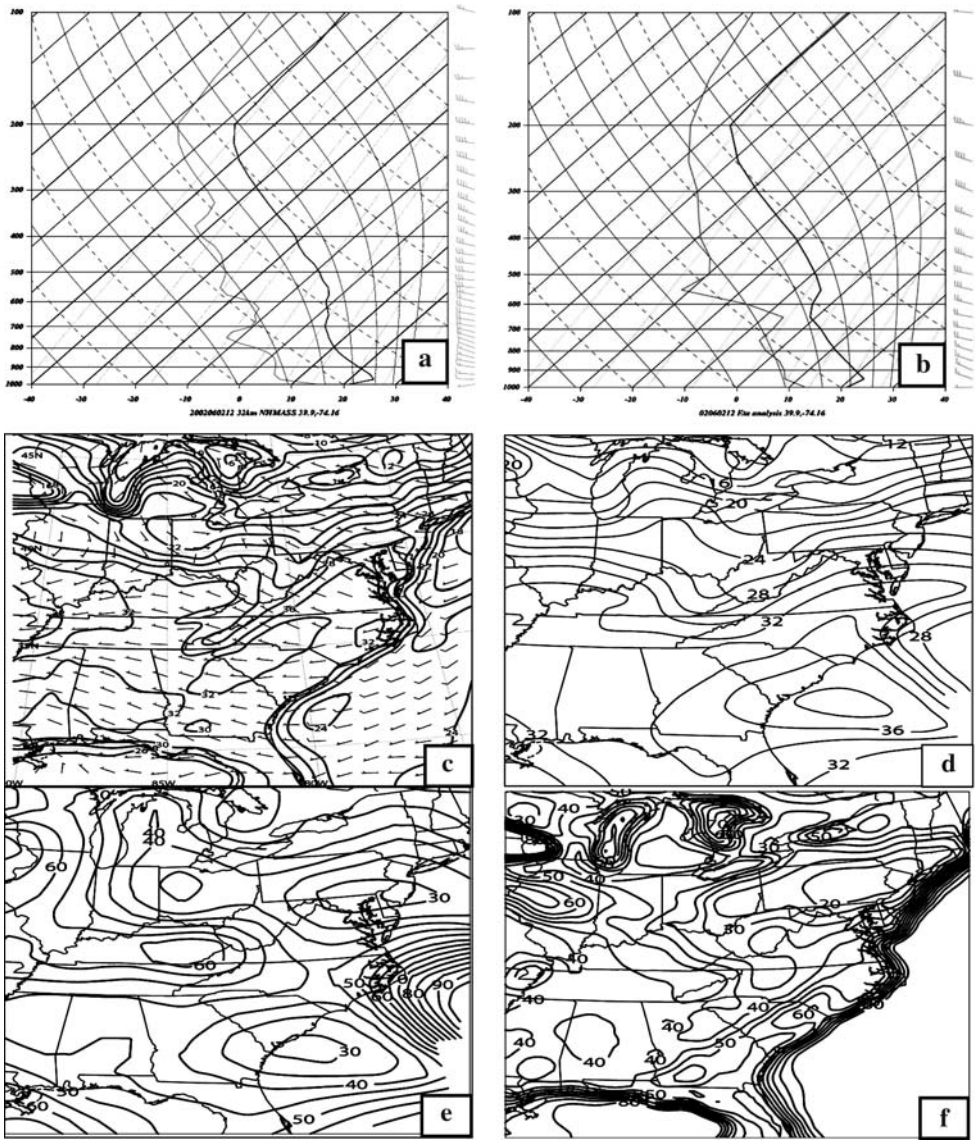

Fig. 12 **a** 32-km simulated sounding valid at DT at 12.00 UTC 2nd June 2002. **b** NWS ETA analysis sounding valid at DT at 12.00 UTC 2nd June 2002. **c** 32-km simulated 1,000-hPa temperature (°C) and wind barbs (short barb 5 m/s and long barb 10 m/s) valid at 18.00 UTC 2nd June 2002. **d** NWS ETA analysis surface temperature (°C) valid at 18.00 UTC 2nd June 2002. **e** NWS ETA analysis surface relative humidity (%) valid at 18.00 UTC 2nd June 2002. **f** 32-km simulated surface relative humidity (%) valid at 18.00 UTC 2nd June 2002. **g** NCEP ETA reanalysis 850-hPa temperature (°C) and wind barbs (short barb 5 m/s and long barb 10 m/s) valid at 18.00 UTC 2nd June 2002. **h** 32-km simulated 850-hPa temperature (°C) and wind barbs (short barb 5 m/s and long barb 10 m/s) valid at 18.00 UTC 2nd June 2002. **i**, **j** Same as **g**, **h** except for 500-hPa temperature. Note the *X* for DT location and *PJ* for the core of the polar jet

4 Numerical model simulations of dual dry surges at DT

4.1 Stage I—basic jet circulation and deep mass adjustments forcing the strengthening of the low-level dry front and *first* PBL dry surge

Figure 13a–c depicts fields that show the 32-km simulated thermally indirect circulation in the jet exit region above the eastern OH–western PA region during the 09.00–12.00 UTC period. Figure 13a and b indicates that the equatorward exit region of the mid-upper tropospheric jet is passing over eastern MI, OH, and western PA at 300–500 hPa during the period from ~09.00 to 12.00 UTC, which is consistent with the NARR-A observations depicted earlier in Fig. 7. The equatorward-directed ageostrophic flow at 09.00 UTC in Fig. 13a over western PA is consistent with the sinking motion in the southwest-northeast-oriented cross section located along a line from near PIT to Ottawa, Ontario (CYOW) at 09.00 UTC in Fig. 13b. It is also consistent with the dry tongues (darkest shading) below 300 hPa in the same cross section in the descending branch of the indirect circulation. Note the downward-directed ageostrophic circulation vectors near the darkly shaded zones in the southern half of this cross section. The simulated parcel trajectory in Fig. 13c indicates the descent of the parcel located over northeastern Wisconsin by 09.00 UTC over southeastern MI by 12.00 UTC and central PA by 15.00 UTC. Warming of the parcel can be seen in Fig. 13c within the descending branch of the secondary circulation. Also notice how the parcel originates at 06.00 UTC on the anticyclonic side, not the cyclonic side of the jet and above the 875-hPa ridge in Fig. 1a over Minnesota. The arrival of convergent, sinking, and drying flow in the middle troposphere over western PA

Fig. 12 continued

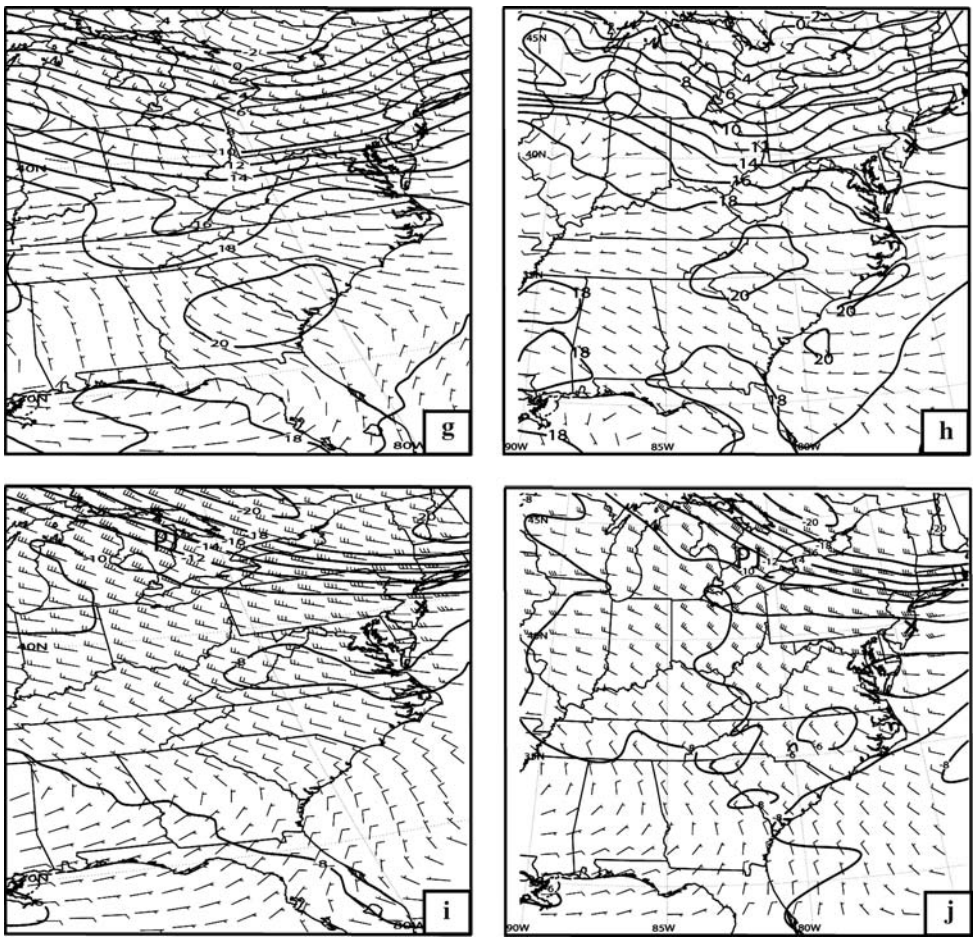

in this simulation is also similar to the NARR-A ageostrophy and sinking at 09.00 UTC and 500 hPa depicted in Fig. 7b and f. The fact that multiple data sources indicate equatorward-directed ageostrophic flow, sinking, and drying over western PA at 09.00 UTC is consistent with observed surface pressure rises over this same region depicted in Fig. 8a. The low-level isallobaric convergence ahead of the pressure rises is followed by low-level isallobaric divergence behind the pressure rises as a result of the velocity variation behind the wind shift line/dry cold front. The resulting moisture flux convergence ahead of the pressure rises is then followed by moisture flux divergence behind the pressure rises. This acts to reduce the low-level moisture values in the divergence behind the wind shift line/dry cold front, as indicated in the surface moisture fields depicted in Fig. 5a and the 875-hPa velocity divergence in Fig. 3d. The simulated isallobaric convergence, "C," followed by divergence "D," in Fig. 13d acts to reinforce the low-level dry cold front's thermally direct circulation by enhancing ascent ahead and descent behind it. The 8-km model 850 hPa isallobaric west and northwesterly wind component (downstream of D in Fig. 13d) is just upstream from the frontal trough (dashed). It is under the equatorward exit region of the jet within this same region of southwestern and south-central PA in between PIT and HAR.

Figure 14 is the key figure in this model simulation section of the paper. It depicts the evolution of the 8-km simulated relative humidity and pressure on the 302-K isentropic surface (Fig. 14a, c, e, g, i, k) relative to 850-hPa winds and heights (Fig. 14b, d, f, h, j, l) from 10.00 to 20.00 UTC. During the early to middle part of this period, one can see important juxtapositions among the 850-hPa height trough (dashed), northwesterly flow (shaded >14 m/s), isentropic pressure ridge perturbations #1 and #2, and relative humidity fields (shaded <25%). Between 10.00 and 12.00 UTC, one can see that, as the west-northwesterly flow just behind the 850-hPa trough strengthens to >17 m/s over the region from south-central to eastern PA, the 302-K pressure ridge (#1 in Fig. 14a, c, e) near ~800 hPa amplifies and is located nearly coincident with the increasing isallobaric northwesterly flow and divergence (D) behind the 850-hPa pressure trough in Fig. 13d. Ahead of the 850-hPa accelerating flow is an isentropic trough or minimum of pressure on 302 K nearly coincident with the 850-hPa trough. Drier relative humidity values between 25 and 50%

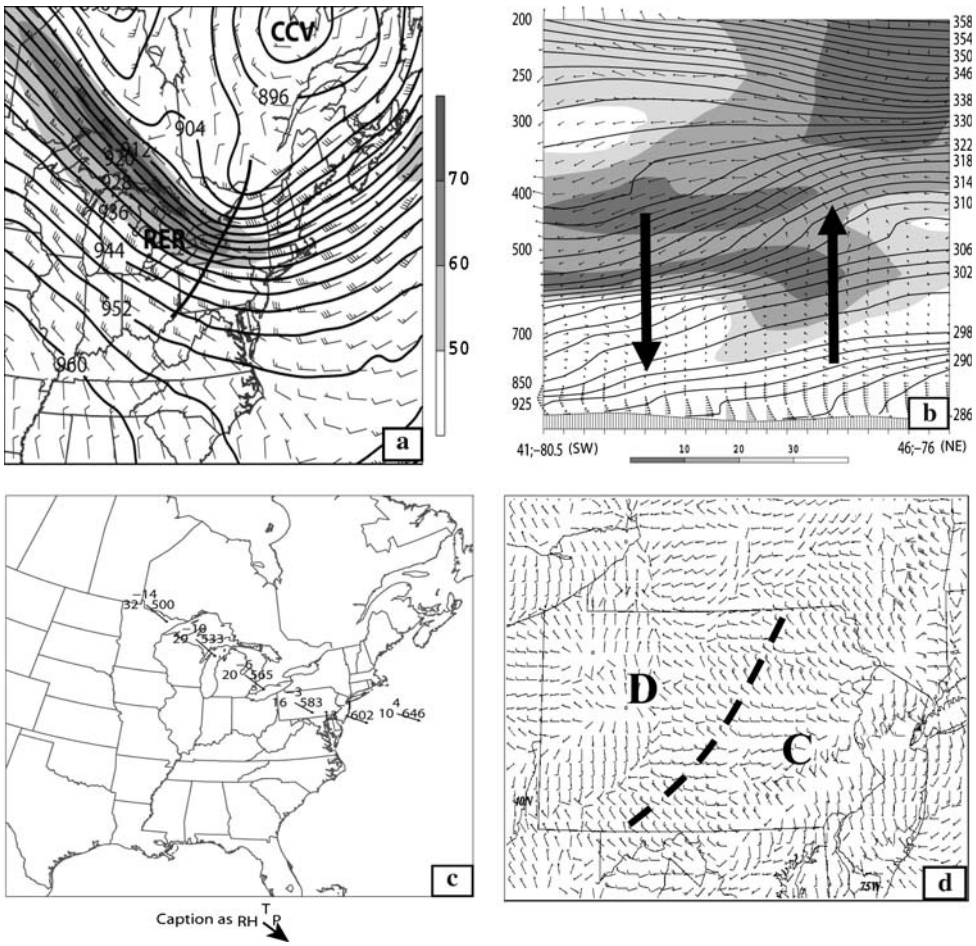

Fig. 13 **a** 32-km simulated 300-hPa total wind isotachs (m/s), wind vectors, and heights (m) valid at 12.00 UTC 2nd June 2002. The *straight line* is the cold trough and the cross section location in **b**, *CCV* is the cold core vortex, and *RER* the right exit region of the total wind jet. **b** 32-km simulated northeast-southwest-oriented vertical cross sections of ageostrophic circulation vectors, potential temperature (K), and relative humidity (shaded in % with darkest shading indicating driest relative humidity <10%) valid at 09.00 UTC 2nd June 2002 from near Ottawa, Ontario (CYWO) to near Pittsburgh, Pennsylvania (PIT). The *arrows* depict the nature of the thermally indirect transverse ageostrophic circulation in the jet exit region. **c** 32-km simulated forward trajectory initialized in the right entrance region of the 500-hPa total wind jet at 06.00 UTC 2nd June 2002 with 3-h location, pressure (hPa), relative humidity (%), and temperature (°C) plotted through to 21.00 UTC 2nd June 2002. **d** 8-km simulated 850-hPa isallobaric wind vectors (m/s), valid from 11.00 to 12.00 UTC 2nd June 2002. The *dashed line* and *C*/*D* represent the transition from isallobaric divergence to convergence

(not shown) accompany isentropic ridge #1, where the isentropes fold downwards. This downfolding ridge (#1) is right behind the 850-hPa and isentropic troughs, where the isentropes fold upwards. Ahead of #1 between 12.00 and 14.00 UTC is a region of moister air where the isentropes extend vertically to ~765 hPa. A region of warming and drying to the west of the 850-hPa trough is located within the mesoscale isentropic ridge (#1). Both this feature with sinking and warming to the west of the 850-hPa trough in the cooler air and the rising and cooling to the east of the 850-hPa trough in the warmer air are consistent with a thermally direct circulation. This circulation propagates southeastwards across NJ, so that by 14.00–16.00 UTC (Fig. 14e–h), the region over DT transitions towards northwesterly flow from westerly flow, decreasing the relative humidity and inducing slightly cooler temperatures near 850 hPa, as indicated in the NARR-A observations, in which cooling and drying occurred at 875 hPa in Fig. 1a–d between 12.00 and 15.00 UTC.

By 16.00 UTC, in Fig. 15a and b is depicted the 8-km simulated vertical motions (cm/s) and relative humidity (shaded <25%) at 800 hPa in which descent has arrived over most of southeastern PA and southern NJ. This descent is consistent with the sinking air behind the 850-hPa trough/wind shift line/dry front (isallobaric divergence below 850 hPa) moving through the region depicted in Fig. 14f, h and j. This is in proximity to the strengthening isentropic ridge (#1) east of the Delaware River Valley extending to just southwest of and eventually offshore of DT in Fig. 14e, g and i. The vertical cross section from

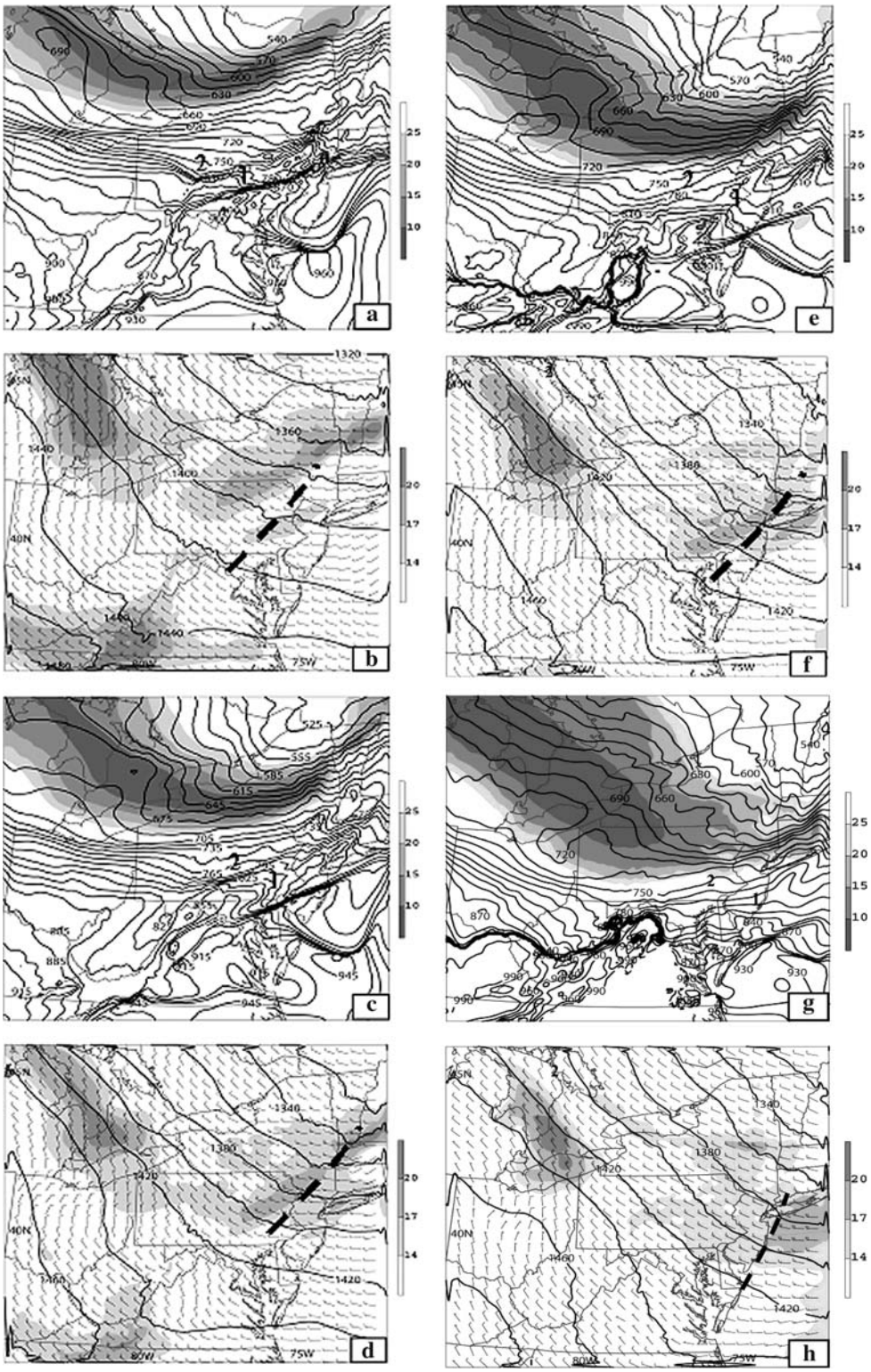

Fig. 14 8-km simulated relative humidity (shaded in % with driest air <10%) and pressure (solid in hPa) on the 302-K isentropic surface and 850-hPa wind barbs, height (solid in m), and isotachs (shaded in m/s with darkest shading being the highest velocity >20 m/s) valid at **a**, **b** 10.00 UTC; **c**, **d** 12.00 UTC; **e**, **f** 14.00 UTC; **g**, **h** 16.00 UTC; **i**, **j** 18.00 UTC; and **k**, **l** 20.00 UTC 2nd June 2002. The *dashed lines* represent the transition zone between northwesterly upstream and westerly downstream flow and the (*1*) near 800 hPa and the (*2*) near 750 hPa are the locations of the two isentropic ridges where drying is most pronounced in sequential episodes. The two levels selected are based on the two regions of drying initially below 800 hPa and later above 750 hPa that eventually couple during stage III

near HAR to near DT at 16.00 UTC in Fig. 15c shows this descent (large downward arrow/#1) and drying (wedge of low-level dark shading) approaching DT from the west as expected from the 800-hPa omega fields in which low-level descending air behind the dry front and within the mesoscale isentropic ridge (#1) is following the ascent ahead of it. During the 16.00–18.00 UTC period, one can see that the horizontal and vertical cross sections depicted in Figs. 14g–j and 15a–c indicate descent arriving in the PBL as the wind shifts to the northwest and the descending

Fig. 14 continued

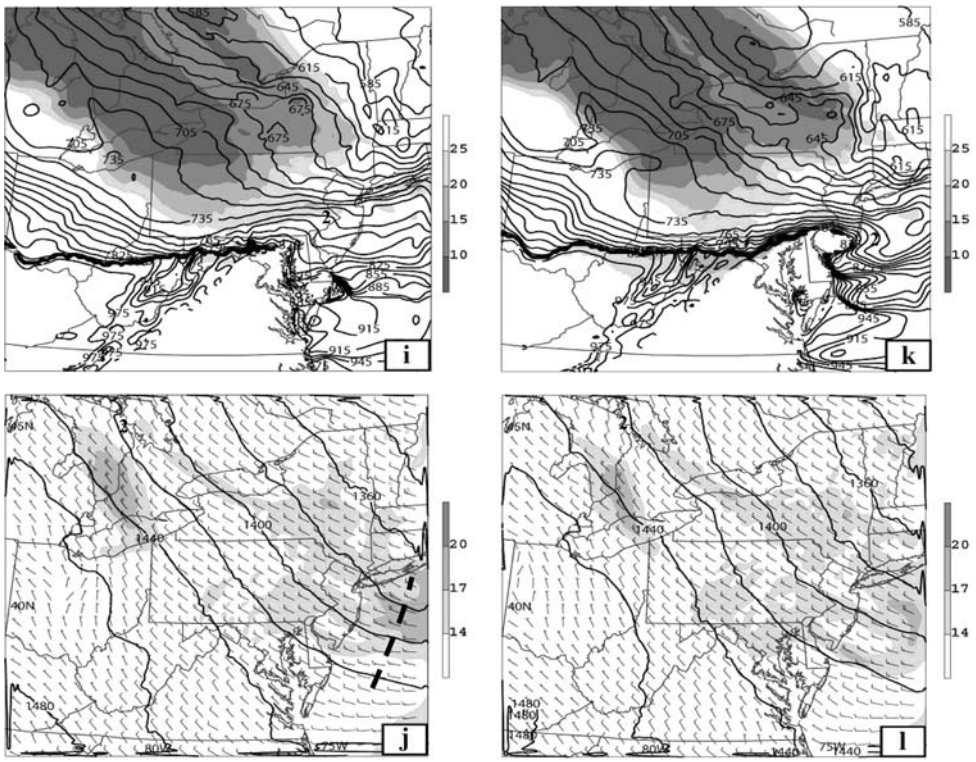

branch of the thermally direct low-level circulation arrives at DT. Cooling near 800 hPa in the 8-km simulated HAR soundings during the period 14.00–16.00 UTC in Fig. 15e and f is also observed in the NARR-A observations, indicating the passage of the PBL front to the east and weak isallobaric cold air advection (Fig. 1c, d). Also evident in this and HAR soundings (Fig. 15c, d) are two distinct dry layers above and below 700 hPa similar to the NARR-A observations in Fig. 6, as well as the KIAD and KPIT rawinsondes in Fig. 10a, b. Note, however, the later drying in the layer surrounding 800 hPa by 16.00 UTC in Fig. 15f at HAR. Thus, as was seen in the asynoptic observations, the first surge of dry air arrives at DT following the trough. This surface dry surge is indicative of a weak surface dry cold front and the low-level thermally direct circulation between 15.00 and 16.00 UTC near DT. The west-northwesterly flow observed at KACY is slightly ahead of these simulated fields, as the model is $\sim$1 h slow. Thus, the dry front is really not heralding in the strongest cool air advection but instead a windshift to the west-northwest from the earlier west-southwest and more pronounced dry air advection in the isallobaric divergence under the descending branch of the thermally direct circulation. This is consistent with the KACY meteogram, New Brunswick wind profiler (not shown), and Sandy Hook GPS, as well as NARR-A sinking and zonal dry air advection $\sim -38 \times 10^{-8}$ kg/kg. The deeper drying signals inferred from the satellite imagery at 16.15 UTC in Fig. 9c, as well as the second dry surge at KACY and Sandy Hook, occur $\sim$1–2 h after this time.

4.2 Stage II—arrival of the mid-upper tropospheric dry surge with the jet exit region circulation

Figure 14g, i, k's simulated 302-K pressure indicates that, between 16.00 and 20.00 UTC, the main pool of dry air on the anticyclonic side of the polar jet exit region propagates south-southeastwards across PA just north of the intersection of the 750-hPa surface with the 302-K surface. Above 750-hPa, a region of progressively drier air with relative humidity <25% (shaded) is oriented west–east and is dropping southward and eastward from eastern PA towards southern NJ as the equatorward exit region of the mid-upper tropospheric jet streak arrives (note Fig. 14g, i, k). This dry tongue originally extends up to $\sim$650 hPa as the 302-K surface slopes upwards into the core of the polar jet streak well upstream over the Great Lakes and Canada, where a plume of relative humidity <20% is aligned with the core and equatorward exit region of the jet as it propagates east-southeastwards. Consistent with earlier depicted water vapor imagery at 15.15 UTC in Fig. 9b, although somewhat slower, between 16.00 and 18.00 UTC, this simulated higher level dry tongue with relative humidity <25% drops southwards, eventually bifurcating into two surges, a narrower west–east swath over eastern PA and central NJ at $\sim$740 hPa approaching DT and a

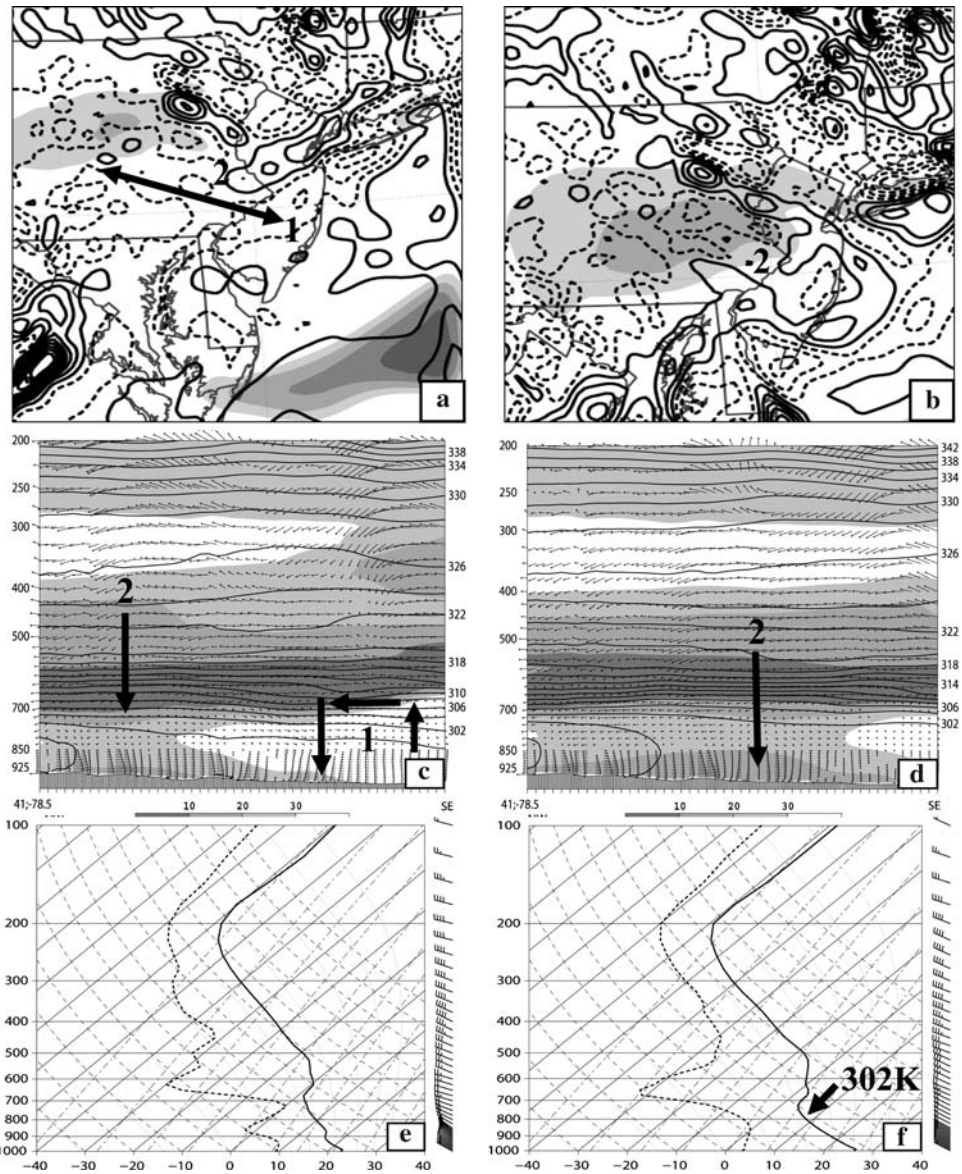

Fig. 15 8-km simulated 800-hPa vertical motion (positive solid beginning at 0 cm/s and negative dashed beginning at −4 cm/s; contour interval is 4 cm/s) and relative humidity (shaded in % with darkest shading relative humidity <10%) valid at **a** 16.00 and **b** 18.00 UTC 2nd June 2002. 8-km simulated vertical cross sections of ageostrophic circulation vectors, potential temperature (solid) and relative humidity (shaded in % with darkest shading relative humidity <10%) from Harrisburg, Pennsylvania (HAR) to DT (*solid line* in Fig. 13a) and valid at **c** 16.00 UTC and **d** 18.00 2nd June 2002. 8-km simulated soundings at HAR valid at **e** 14.00 UTC and **f** 16.00 UTC; (*1*) and (*2*) as in Fig. 14. The *thick arrows* emphasize the ageostrophic circulation

poleward dry surge to the northeast above 650 hPa over upstate New York. The equatorward dry surge arriving near DT is almost 60 hPa higher than the first dry tongue that arrived over southern NJ ~2 h earlier accompanying the 850-hPa trough and isentropic ridge at 800 hPa (#1). This second (equatorward) surge of dry air to arrive near DT (accompanying isentropic ridge #2, which followed ridge #1) clearly has descended from over eastern Ohio to south-central and southeastern PA in the equatorward exit region's thermally indirect circulation, consistent with the bifurcating features depicted in Fig. 14g, i and k. This is equatorward of the conveyor belt of colder air descending from over northern PA and NY, i.e., south of the (poleward) dry surge and observed descending IPV maximum/tropopause fold (not shown). The 8-km simulated backward trajectory depicted in Figure 16a launched at 18.00 UTC near DT shows the descent through 680 hPa of the air from the northwest then the west that originated near 600 hPa north of Lake Erie at 12.00 UTC just northwest of the jet exit region vertical cross section in Fig. 13b. Note the confluent structure inferred from the trajectories in Figs. 13c and 16a after 15.00 UTC over southeastern PA and southern NJ. Such confluent flow is consistent with the secondary circulation and second isentropic ridge (#2 in Fig. 14g–k during the period 16.00–20.00 UTC) that amplifies and builds eastward at 750 hPa from over south-central PA to the east of DT. This isentropic ridge (#2) flanks the jet's equatorward exit region and the confluence associated with the trajectories in Figs. 13c and 16a, which allow dry air to descend to below 750 hPa in between the Delaware River and DT. This dry air surge is equatorward of the very cold air over upstate NY (poleward dry surge).

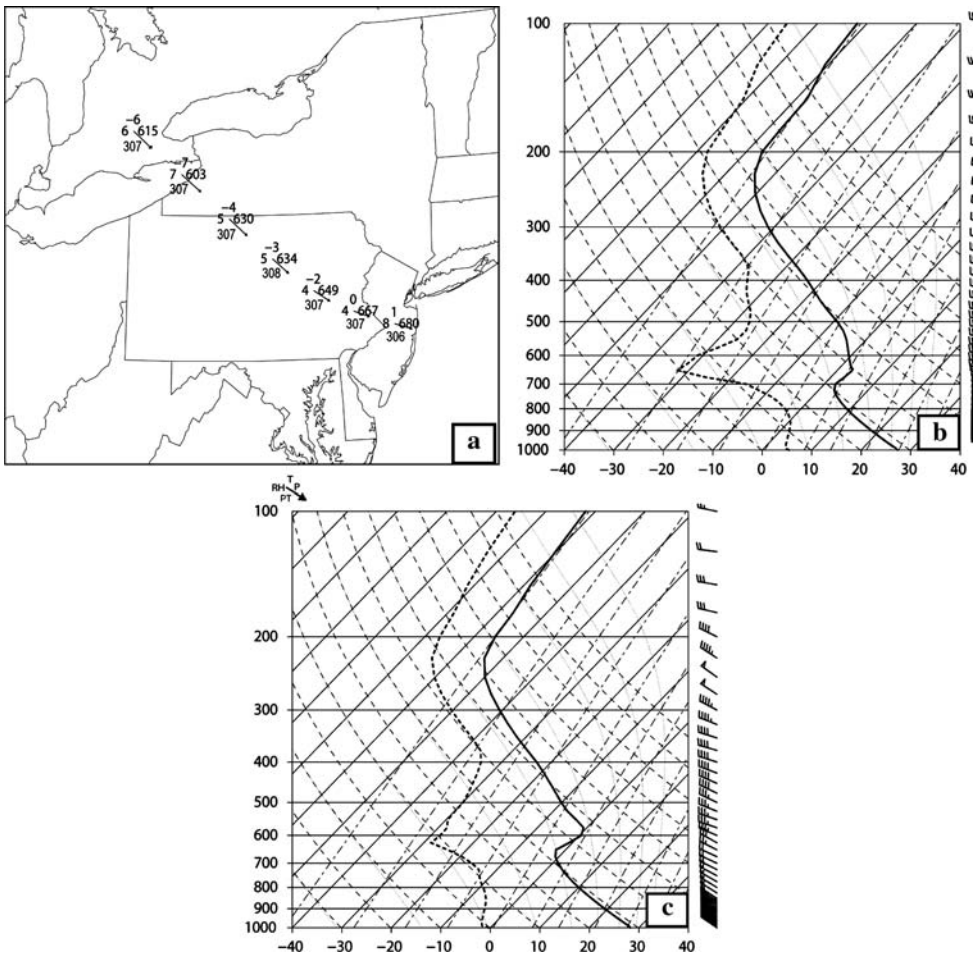

Fig. 16 **a** 8-km simulated backward trajectory initialized just northwest of DT at 18.00 UTC 2nd June 2002 at ~680 hPa backward to its location at 12.00 UTC with hourly location, potential temperature (K), pressure (hPa), relative humidity (%), and temperature (°C). **b**, **c** 2-km simulated soundings at DT valid at 18.00–20.00 UTC 2nd June 2002

Note the signal of this transport in the drying in the 2-km simulated soundings at DT in Fig. 16b and c in between 700 and 850 hPa during the 18.00–20.00 UTC time period.

4.3 Stage III—mixing of the jet dry air surfaceward in the convective PBL, resulting in the *second* surface dry air surge

Figure 14g, i, k depict the spreading of the blank (white) area from the southwest-northeast during the 16.00–20.00 UTC time period, indicating the vertical 302-K isentrope or dry adiabatic lapse rate below 700 hPa (note also the arrow in Fig. 15d (#2) and lapse rate in Fig. 16c below 700 hPa). This white area includes a narrow strip from northern VA through southeastern PA, MD, and southern NJ by 20.00 UTC approaching DT. This is collocated with the simulated bifurcated drying arriving from PA to over DT by 18.00 UTC above 750 hPa (near isentropic ridge #2). Consistent with these signals are the DT 2-km simulated soundings in Fig. 16b and c, which shows the deepening of the adiabatic layer and the development of a more uniform and deeper dry layer from the mid-troposphere to the surface, thus, erasing the earlier dual dry layers. Note the simulated ~30°C surface dewpoint depression and temperature ~29°C at 20.00 UTC (with no decrease in surface temperature between 18.00 and 20.00 UTC) in Fig. 16c. This should be compared to the observed surface temperature at 18.00 UTC at KACY of ~29°C and dewpoint depression ~26°C in Fig. 2b (also with virtually no decrease in surface temperature between 16.00 and 18.00 UTC). Thus, the second surge of dry air arrives in the simulation near DT, albeit 1–2 h late relative to the observations. This is a signal of the coupling of the descent in the #2 isentropic ridge accompanying the equatorward jet exit region circulation above 750 hPa, with the diurnal heating of the PBL extending east-northeastwards from northern VA to southwestern NJ between 16.00 and 20.00 UTC. NARR-A PBL heights indicated an impressive deepening from ~1,200 to ~2,100 to ~2,250 m during the 15.00–18.00–21.00 UTC periods, respectively, just kilometers west-northwest of DT, confirming deep mixing during the second drying period. NARR-A sinking motions at and above 725 hPa produce drying within the PBL at a rate >~0.001 kg/kg reduction in specific humidity per hour above the strongest turbulent mixing, making that air available for surface drying.

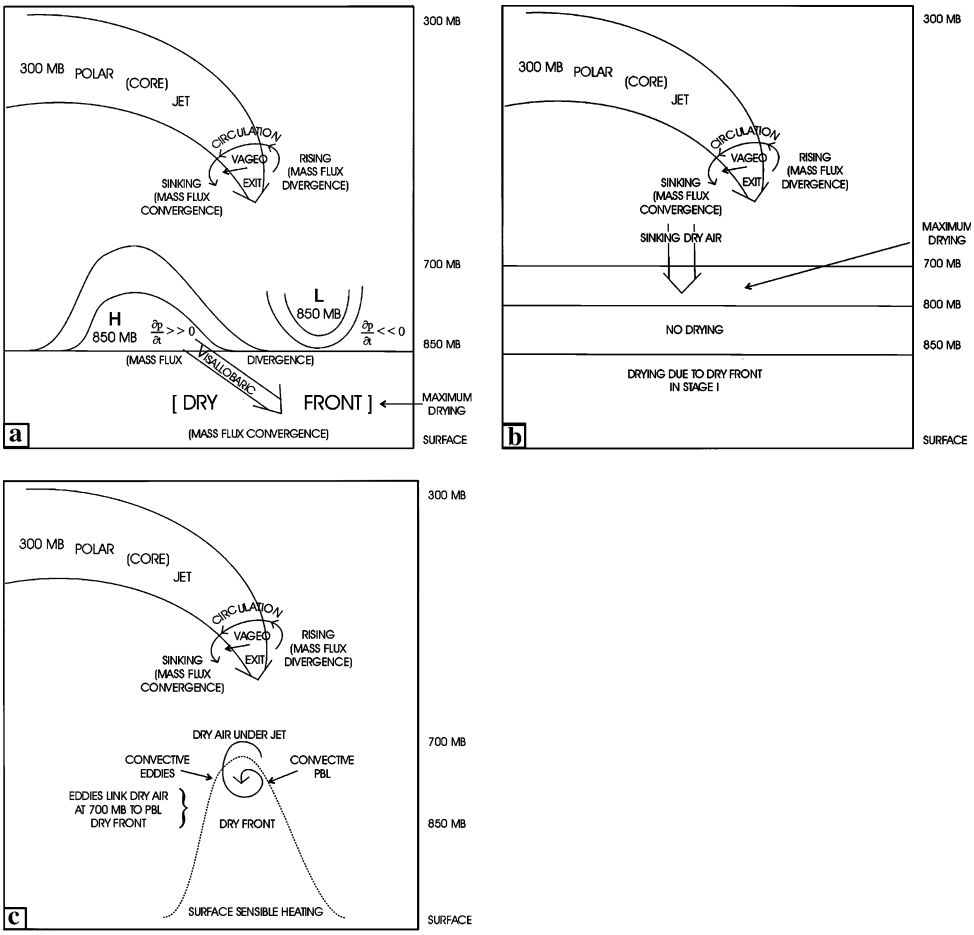

Fig. 17 Three-stage fire weather paradigm

It is also consistent with the narrow "black" area (southern arrow indicating equatorward dry surge) depicted in the water vapor imagery in Fig. 9c that develops by 16.15 UTC in between northern VA and DT in contrast to the "black" area over upstate NY (northern arrow indicating poleward dry surge likely within a cold conveyor belt and under a tropopause fold).

In summary, the NHMASS model-simulated multi-scale processes leading to dual dry surges observed near DT can be described in terms of a three-stage paradigm. During stage I, the equatorward exit region of the mid-upper tropospheric jet streak propagates southeastwards from the Great Lakes to PA, producing sinking and pressure rises under its thermally indirect circulation. As the pressure, rises under the equatorward exit region, there is a southeastward-directed isallobaric wind component, which develops in the lower troposphere. The northwesterly accelerating boundary layer flow under this region of mid-upper tropospheric velocity convergence and low-level cold air advection sustains a PBL dry front. This low-level dry front contains a thermally direct circulation and descending dry air in the isallobaric divergence zone just behind the front. This represents the first surge of dry air to arrive at the location of the DT fire around 15.00–16.00 UTC. Stage II occurs as dry air aloft under the equatorward exit region of the jet propagates southeastwards just upstream from the boundary layer dry tongue accompanying the low-level dry front in stage I. This upper-level dry air surge descends to $\sim$725 hPa, but is not, at first, directly coupled to the PBL dry surge at DT. Stage III follows as surface sensible heat flux behind the PBL dry front in the low-level northwesterly flow thickens the convective PBL to $\sim$2.5 km in depth, forcing the mixing of dry air under the jet streak aloft into the PBL (linking the air below 800 hPa to the air above 750 hPa), thus, inducing another drying episode after 18.00 UTC at and surrounding DT.

5 Summary and conclusions

In-depth observational and numerical model-generated fields have been employed to diagnose the processes responsible for anomalous surface drying prior to a blowup fire event. The fire occurred far downstream and equatorward from the entrance region of a jet streak and its

tropopause fold, which is often associated with the extreme transport of dry air into the planetary boundary layer (PBL). Additionally, it occurred equatorward and southwest of Carlson's (1980) cold conveyor belt, as the dry air from the surface through 650 hPa emanated not from the cold pool flanking a deep cyclone, but well southwest of that airstream. As has been observed in the past, the drying in this case accompanied a weak surface cold front under a broad trough aloft and within the exit region of an anticyclonically curved mid-upper tropospheric jet streak located just upstream.

The observationally diagnosed and Non-Hydrostatic version of the Mesoscale Atmospheric Simulation System (NHMASS) model-simulated multi-scale processes leading to dual dry surges observed near DT can be described in terms of a three-stage paradigm (note Fig. 17). During stage I (Fig. 17a), the equatorward exit region of the mid-upper tropospheric jet streak propagates southeastwards from the Great Lakes to NJ, producing sinking and pressure rises primarily below 800 hPa under its thermally indirect circulation. The upper-level convergence phases with low-level cold air advection to further intensify the low-level isallobaric wind. As the pressures rises under the equatorward exit region, there is a southeastward-directed isallobaric wind component, which develops in the lower troposphere. The northwesterly accelerating boundary layer flow under this region of convergence aloft sustains a PBL dry front with a thermally direct circulation and descending dry air in the isallobaric divergence zone just behind the surface cold front and trough. This represents the first surge of dry air to arrive at the location of the DT fire around 15.00–16.00 UTC, with both strong low-level descent and primarily zonal dry air advection contributing to $\sim 1 \times 10^{-2}$ kg/kg reduction in specific humidity per hour.

Stage II (Fig. 17b) occurs as dry air aloft under the equatorward exit region of the jet propagates southeastwards just upstream from the boundary layer dry tongue accompanying the low-level dry front in stage I. This upper-level dry air surge descends to ~ 725 hPa and bifurcates away from the jet in the confluent flow but is not, at first, directly coupled to the PBL dry surge at DT.

Stage III (Fig. 17c) follows as surface sensible heat flux behind the PBL dry front thickens the convective PBL up to ~ 2.5 km, forcing the mixing of dry air (under the sinking within the jet streak aloft that commenced during stage II) into the convective PBL, thus, inducing another drying episode after 18.00 UTC southwest of and surrounding DT.

From a broader perspective, the aforementioned multi-scale processes likely describe a mechanism for deep vertical exchange under the equatorward exit region of a mid-upper tropospheric jet streak or "equatorward dry surge." Critical for the exchange is the thickening of a convective PBL in the right place at the right time. This is facilitated by strong surface sensible heat flux and cooling within the middle-lower troposphere. The evidence supports the fact that low-level equatorward drying begins well upstream of the lee slope of the mountains and well equatorward and west of the cold conveyor belt and tropopause fold to the north and northeast (poleward drying). This indicates the importance of the coupling among the low-level thermally direct, upper-level thermally indirect, and well-mixed PBL circulations in producing the rapid/extreme drying observed in the prefire environment. While this occurs for one dramatic case study, it is important that additional investigations of other case studies of explosive drying are undertaken to ascertain the order and magnitude of these processes in differing configurations of synoptic scale features and terrain.

Acknowledgments This research was funded by the USDA Forest Service under grant #02-JV-112313000-051. Phillip Marzette, Chris Adaniya, and Kristien King of the University of Nevada, Reno, modified the electronic figures for publication. David Stettner of CIMMS at the University of Wisconsin provided the water vapor satellite imagery. The surface and rawinsonde observations were derived from the Plymouth State University Weather Center web site.

References

Brotak EA, Reifsnyder WE (1977) An investigation of the synoptic situations associated with major wildland fires. J Appl Meteor 16:867–870

Carlson TN (1980) Airflow through midlatitude cyclones and the comma cloud pattern. Mon Wea Rev 108:1498–1509

Charney JJ, Bian X, Potter BE, Heilman WE (2003) Mesoscale simulations during the Double Trouble State Park wildfire in east-central New Jersey. In: Proceedings of the 10th AMS Conference on Mesoscale Meteorology, pp 2–13

Danielsen EF (1968) Stratospheric-tropospheric exchange based on radioactivity, ozone and potential vorticity. J Atmos Sci 25:502–518

Kaplan ML, Lin Y-L, Charney JJ, Pfeiffer KD, Ensley DB, Weglarz RB, DeCroix DS (2000) A terminal area PBL prediction system at Dallas—Fort Worth and its application in simulating diurnal PBL jets. Bull Am Meteor Soc 81:2179–2204

Kondo J, Kuwagata T (1992) Enhancement of forest fires over northeastern Japan due to atypical strong dry wind. J Appl Meteor 31:386–396

Mesinger F, DiMego G, Kalnay E, Shafran P, Ebisuzaki W, Jovic D, Woollen J, Mitchell K, Rogers E, Ek M, Fan Y, Grumbine R, Higgins W, Li H, Lin Y-L, Manikin G, Parrish D, Shi W (2006) North American regional reanalysis. Bull Am Meteor Soc 87:343–360

Mills GA (2005a) A re-examination of the synoptic and mesoscale meteorology of Ash Wednesday 1983. Aust Met Mag 54:35–55

Mills GA (2005b) On the sub-synoptic scale meteorology of two extreme fire weather days during the eastern Australia fires of January 2003. Aust Met Mag 54:265–290

New Jersey State Forest Fire Service (NJFFS) (2003) Division forest firewardens report of large fire and problem fire analysis: Jakes Branch Wildfire B06-02-02 (2002), pp 20

Schultz DM (2001) Reexamining the cold conveyor belt. Mon Wea Rev 129:2205–2225

Simard AJ, Haines DA, Blank RW, Frost JS (1983) The Mack Lake fire. USDA Forest Service General Technical Report NC-83, North Central Research Station (NCRS), pp 40

Therry G, Lacarrère P (1983) Improving the eddy kinetic energy model for planetary boundary layer description. Boundary-Layer Meteor 25:63–88

Uccellini LW, Johnson DR (1979) The coupling of upper and lower tropospheric jet streaks and implications for the development of severe convective storms. Mon Wea Rev 107:682–703